International
Progress Report

IPR-01-63

Äspö Hard Rock Laboratory

Prototype Repository

Geoelectric Monitoring in Buffer, Backfill and Rock

T Rothfuchs
M Komischke
R Miehe
H Moog
K Wieczorek

Gesellschaft für Anlagen- und Reaktorsicherheit (GRS) mbH

August 2001

Svensk Kärnbränslehantering AB
Swedish Nuclear Fuel
and Waste Management Co
Box 5864
SE-102 40 Stockholm Sweden
Tel +46 8 459 84 00
Fax +46 8 661 57 19

Äspö Hard Rock
Laboratory

Report no.	No.
IPR-01-63	F63K
Author	Date
Rothfuchs, Komischke, Miehe, Moog, Wieczorek	01-08-31
Checked by	Date
Roland Pusch	01-11-15
Approved	Date
Christer Svemar	02-03-27

Äspö Hard Rock Laboratory

Prototype Repository

Geoelectric Monitoring in Buffer, Backfill and Rock

T Rothfuchs
M Komischke
R Miehe
H Moog
K Wieczorek

Gesellschaft für Anlagen- und Reaktorsicherheit (GRS) mbH

August 2001

Keywords: Prototype Repository, Geoelectric monitoring, buffer, backfill, GRS

PROTOTYPE REPOSITORY

PROTOTYPE REPOSITORY

Deliverable D 9

Geoelectric Monitoring in Buffer, Backfill and Rock

T Rotfuchs
M Komischke
R Miehe
H Moog
K Wieczorek

Gesellschaft für Anlagen- und Reaktorsicherheit (GRS) mbH

August 2001

EC Contract FIKW-2000-00055

EC-5th EURATOM Framework programme 1998-2002
Key Action: Nuclear Fission

1 Abstract

The resistivities of the original buffer material have been found to be similar to those of the less smctitic backfill. This can be explained by a clay-typical interface conductivity which is due to additional cations held loosely in the diffuse part of the electrical double layer surrounding the clay particles. Even a small amount of solution leads to formation of a double layer and causes the interface conductivity.

The buffer and backfill have a rather low initial resistivity, which in conjunction with the comparably high resistivity of the rock, implies that further resistivity reduction by increasing water content of the buffer cannot be accurately detected if the electrodes are located in the rock or rather close to the rock. This has called for changes in the electrode arrangement in the drift.

Besides its dependence on the water content, the electrical resistivity is also a function of salinity and composition of the pore solution. Since both may change as the solution penetrates the buffer and the backfill, investigations were performed in order to quantify this effect.

2 Sammanfattning

Det elektriska motståndet hos buffertmaterialet har visat sig likna motståndet hos den smektitfattigare återfyllningen. Det kan förklaras av en för leror typisk ytrelaterad konduktivitet som beror på ett överskott av katjoner som hålls löst bundna i det diffusa elektriska dubbellager som omger partiklarna. Också en ringa lösningsmängd räcker för att bilda dubbellagren och orsaka ytledning.

Buffert- och återfyllningsmaterialen har ett relativt lågt initiellt elektriskt motstånd, vilket tillsammans med ett jämförelsevis högt motstånd hos berget innebär att ytterligare motståndsminskning vid ökad vattenhalt inte kan mätas med någon noggrannhet om elektroderna placeras i berget eller nära intill berget. Detta har krävt ändrade planer för elektrodarrangemanget.

Förutom beroendet av vattenhalten är det elektriska motståndet också en funktion av salthalt och porvattenkemi. Eftersom båda kan förändras då en lösning tränger in i buffert och återfyllning har kvantifiering av denna effekt gjorts.

Table of Contents

List of Figures

List of Tables

3 Introduction

Within the framework of the Prototype Repository Project performed by the Svensk Kärnbränslehantering AB (SKB) at the Aespoe Hard Rock Laboratory (HRL) in Sweden six copper casks containing electrical heaters will be emplaced in deposition boreholes drilled into the floor of a drift at 460 m depth below ground. The gap between the casks and the granitic rock will be filled with Na-bentonite buffer. The drift above the deposition boreholes will be backfilled, too with a mixture consisting of 30 % bentonite and 70 % crushed rock.

The rock, buffer and backfill will be instrumented by SKB for recording temperatures, swelling and water pressures. In addition to that, multi-electrode arrays will be installed by the Gesellschaft für Anlagen- und Reaktorsicherheit (GRS) at the top of one deposition borehole, in the drift above the deposition boreholes, and in the rock between two of the deposition boreholes in order to determine water uptake in buffer and backfill and desaturation of the rock by geoelectrical measurements.

In the geoelectric measurements advantage is taken of the dependence of the electrical resistivity in rocks on the water (solution) content. In order to interpret measured resistivity in terms of water content, the field measurements are accompanied by laboratory calibration tests.

Besides its dependence on the water content, the electrical resistivity is also a function of salinity and composition of the pore solution. Since both may change as the solution penetrates the buffer and the backfill, respective laboratory investigations were performed in order to quantify this effect.

On basis of the results of the laboratory investigations model calculations have been performed to determine the achievable measuring resolution and to determine optimized electrode configurations in the surveyed areas.

At the time of the writing of this report about 80 % of the laboratory investigations have been completed. The final layout of the electrode arrays in the drift has been agreed and the installation of the first measurement array will take place in October 2001.

4 Theoretical Principles

In direct current geoelectrics, a stationary electric field is generated in a dielectric by means of two current electrodes and is measured with two further potential electrodes.
In an isotropic medium, the current density J generated by an electric field E is described by the constitutive equation (Ohm's law),

$$J = \sigma E \qquad (1)$$

With the exception of laboratory measurements on test samples of known geometry, the electrical conductivity σ is not directly measurable. The value determined by field measurements depends on the geometry of the measuring arrangement and is affected by the inhomogeneity of the structure; it is therefore designated as the apparent electrical conductivity. In practice, the electrical resistivity, that is, the reciprocal of the conductivity, is more frequently employed and is denoted by $\rho = 1/\sigma$.
Since the magnetic field does not vary in the case of a uniform electric current, the following applies:

$$\partial B / \partial t = 0 \qquad (2)$$

From Maxwell's equations, it thus follows that rot E vanishes:

$$\mathrm{rot}\, E = 0 \qquad (3)$$

Equation (13) indicates that E can be expressed as the gradient of a scalar potential ψ:

$$E = -\mathrm{grad}\, \psi \qquad (4)$$

This potential is sufficient because $\mathrm{div}\, J = \mathrm{div}\, (\sigma E)$ in the differential equation:

$$\sigma\, \mathrm{div}\, \mathrm{grad}\, \psi = -\mathrm{div}\, J \qquad (5)$$

In accordance with Gauss' theorem of vector analysis, the volume integral of the divergence of the current density J over the volume V is equal to the sum of the current sources within the volume V:

$$\int_V \mathrm{div}\, J\, dV = I\delta \qquad (6)$$

δ is the Dirac delta function, which assumes the value 1 where sources are present and is otherwise equal to zero. For an infinitesimally small volume dV, the following applies:

$$\mathrm{div}\, J = I\delta \qquad (7)$$

In accordance with (5),

$$\mathrm{div}\, J = -\sigma\, \mathrm{div}\, \mathrm{grad}\, \psi \qquad (8)$$

applies; hence, Poisson's differential equation is finally obtained for the potential field due to arbitrary current sources:

$$\mathrm{div}\, \mathrm{grad}\, \psi = -\rho I\delta \qquad (9)$$

with $\rho = 1/\sigma$.
If it is assumed that the electric field is stationary, E can be derived as an irrotational vector from a potential ψ. If the divergence is determined from (4), the following inhomogeneous potential equation is obtained for ψ:

$$\mathrm{div}\, \mathrm{grad}\, \psi = -\mathrm{div}\, E \qquad (10)$$

The right-hand side of this equation is known. With the application of Green's theorem from vector analysis, ψ can be calculated in the following form:

$$4\pi\psi = \int_V \frac{\mathrm{div}\, E}{r}\, dV \qquad (11)$$

With the use of equations 11, 10, and 9, the potential field ψ is thus obtained for a point source:

$$\psi = \frac{1}{4\pi} I\rho \frac{1}{r} \qquad (12)$$

I is the current which flows through the source, and r is the distance of the point under consideration from the source point for which ψ is being calculated and over whose coordinates the integration is being performed. The source point is also the location of the volume element dV. The potential field of a dipole source results from the superposition of the potential fields for two point sources with positive and negative current:

$$\psi = \psi_1 + \psi_2 = \frac{1}{4\pi} I\rho \left(\frac{1}{r_1} - \frac{1}{r_2} \right) \qquad (13)$$

r_1 and r_2 denote the distances of the points under consideration from source points 1 and 2, respectively, with the potential fields ψ_1 and ψ_2. The potential field generated by the dipole source is measured as a potential difference at two potential electrodes. If equation (13) is applied at each potential probing point, and if the difference is calculated, the following is obtained:

$$\Delta\psi = \frac{1}{4\pi} I\rho \left(\frac{1}{r_{11}} - \frac{1}{r_{12}} - \frac{1}{r_{21}} + \frac{1}{r_{22}} \right) \qquad (14)$$

r_{ij} is the distance of the ith potential electrode from the jth current electrode. The expression between brackets is denoted by 1/K for brevity. K is designated as a geometric factor.
During a measurement, the potential difference as well as the current supplied are measured, and the resistance is determined. This value is the sum of the resistances between the current electrodes and the contact resistances at the electrodes; it is an apparent resistance. The true resistivity is equal to the apparent resistivity only in a homogeneous medium. The apparent resistivity is given by:

$$\rho = 4\pi \frac{\Delta\psi}{I} K \qquad (15)$$

In geoelectrics, a wide variety of electrode arrangements are employed. The Wenner arrangement is worthy of special mention; in this four-point arrangement with equal electrode spacing a, the electrodes lie in a straight line. The outer electrodes are the current electrodes, and the inner electrodes are the potential electrodes. Since $r_{11} = r_{22} = a$ and $r_{12} = r_{21} = 2a$ apply, equation (14) yields the geometric factor as follows:

$$K = \frac{1}{\frac{1}{r_{11}} - \frac{1}{r_{12}} - \frac{1}{r_{21}} + \frac{1}{r_{22}}} = a \qquad (16)$$

In this expression, a is the electrode spacing in a Wenner arrangement.
As a rule, geoelectrics is applied on profiles at the earth's surface, where the factor 4π (three-dimensional space) in (15) is replaced by the factor 2π (half-space); that is, the problem under investigation is two-dimensional. In three-dimensional space, the electrodes are spatially distributed, either in an array on the surface or in boreholes. Special care is necessary for the calculation of the geometric factor, since it may possess poles, which must be taken into account during the measurements.

5 Field Measurements

5.1 Measuring Techniques

The technique most frequently applied for geoelectric measurements in the field is the four-point method (Figure 5-1). An electric current is supplied to the formation at two electrodes. The magnitude and direction of the resulting electric field are dependent on the conductivity conditions in the rock. The measurements are performed by means of a further pair of electrodes; for this purpose, the difference between the potentials at the electrodes is determined. The input electrodes (C1, C2) and the output electrodes (P1, P2) are arranged as single dipoles (Figure 5-1). For a complete data set, the position of the input dipole is fixed and the output dipole is moved around the area to be investigated. Afterwards, the input dipole is moved to another position, and the measurements are repeated. From the measured potential difference (voltage) and the imposed current, the value of the electrical resistivity is obtained in accordance with Ohm's law, with due consideration of the relative position of the four electrodes with respect to one another.

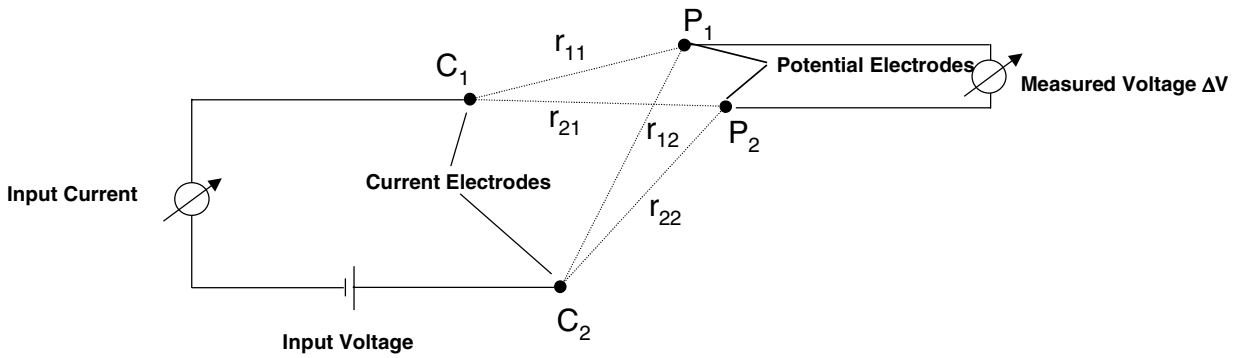

$$\Delta V = \frac{1}{4\pi} I\rho\left(\frac{1}{r_{11}} - \frac{1}{r_{12}} - \frac{1}{r_{21}} + \frac{1}{r_{22}}\right) \qquad (17)$$

Figure 5-1: *Principle configuration of a dipole-dipole measurement*

Although methods of direct current geoelectrics are employed for the evaluation of geoelectric measurements, modern resistivity meters use low-frequency alternating current rather than direct current. The reasons are:

Direct current would cause electrolytic polarization, i. e. build-up of ions around the electrodes. This is prevented by periodic reversal of the current.

Telluric currents, i. e. natural electric currents in the ground, can be accounted for in the measurements when the current is reversed and the measurement results are averaged, since the telluric currents do not change their polarity.

5.2 Measurement Evaluation

For calculating the resistivity, it is assumed that the zone encompassed by the four electrodes is homogeneous. Otherwise, the calculated resistivity value is an apparent resistivity. If various four-point arrangements are employed in a multi-electrode network, the electrical properties can be determined for individual partial zones, which may also overlap. The true resistivity values are determined from the apparent values by means of inverse modelling.
GRS uses the commercial software package RESITOMO (HarbourDom 1996) which allows a 2-dimensional inversion of the measured apparent resistivity data. The RESITOMO-software applies a **m**ultiplicative **s**imultaneous **i**nversion **r**econstruction **t**echnique (MSIRT) which is slightly modified for the resistivity inversion.
Measurement System
All geoelectric systems employed by GRS use low-frequency alternating current. Typically, 2 to 5 current cycles are injected during a single measurement. The period of a cycle is usually between 5 and 10 seconds. Such low frequencies are necessary in order to be able to treat the measurements as direct current geoelectrics; higher frequencies may result in phase differences between injected current and measured voltage. The injected current is in the range between 1 and 200 mA.
RESECS is a PC-controlled DC-resistivity monitoring system for high resolution tomography and other geoelectric applications. The RESECS measuring program runs under MS-Windows98. Up to 240 electrodes are separately addressable by unique decoder addresses. Any pair of electrodes might be selected as current injector. Up to six other pairs of electrodes might serve as potential electrodes for simultaneous geoelectrical measurements (six channel operation). The software controlled fast switching of electrodes results in a high data acquisition rate - up to a few thousands data points per hour.
Features of the stand-alone system are its flexible usage and its convenience in creating geoelectrical standard configurations (Wenner, Schlumberger, Dipole-Dipole etc.) as well as user-defined configurations for multi channel applications. All measuring parameter input is menu-driven.
In measuring mode RESECS automatically selects all programmed electrode configurations. It optimizes preamplification, corrects self potentials and yields DC- resistivity (rho, U, I) as well as IP-values (phaseshift, chargeability). For standard configurations pseudosections and pseudodepth slices are displayed simultaneously. Current injection and its resulting potential differences are displayed online and can be stored on harddisk for later processing.

5.2.1 Hardware Components

All system components are integrated in a 24 height units (HU) 19"-enclosure. The protection rating of the enclosure is IP54. The system is mounted on 4 twin swivel castors.

The front panel and rear panel of the system are illustrated in figures 1 and 2 respectively.

The RESECS resistivity meter essentially consists of the following components:

- Resistivity meter and embedded PC
- Injection voltage supply
- Electrode decoder array
- Uninterruptable power supply

5.2.2 Resistivity Meter and Embedded PC

The resistivity meter and the embedded PC are mounted in a 19"-chassis. It is internally connected to the other components of the system.

The resistivity meter is controlled by the embedded PC. Up to six potential differences are measured simultaneously. Each analog input signal (injection current, potential differences) is supplied with a separate signal path. These signal paths are galvanically isolated from each other and from the embedded PC as well. Each one consists of high quality amplifiers (for impedance adaption, programmable gain setting and isolation), optocouplers and DC/DC converters for the separation of power supplies. Furthermore each signal path is supplied with a DC-accurate, tunable linear phase 5th order Bessel lowpass filter. The cutoff frequencies are software selectable. The AD-converter has a resolution of 16 bit and a conversion interval of 1 ms for each channel.

The injection voltage is switched using a full bridge consisting of high voltage transistors (FET). The switching timing is defined by software.

The electrode address code is created electronically by converting digital PC output to a serial function and address code.

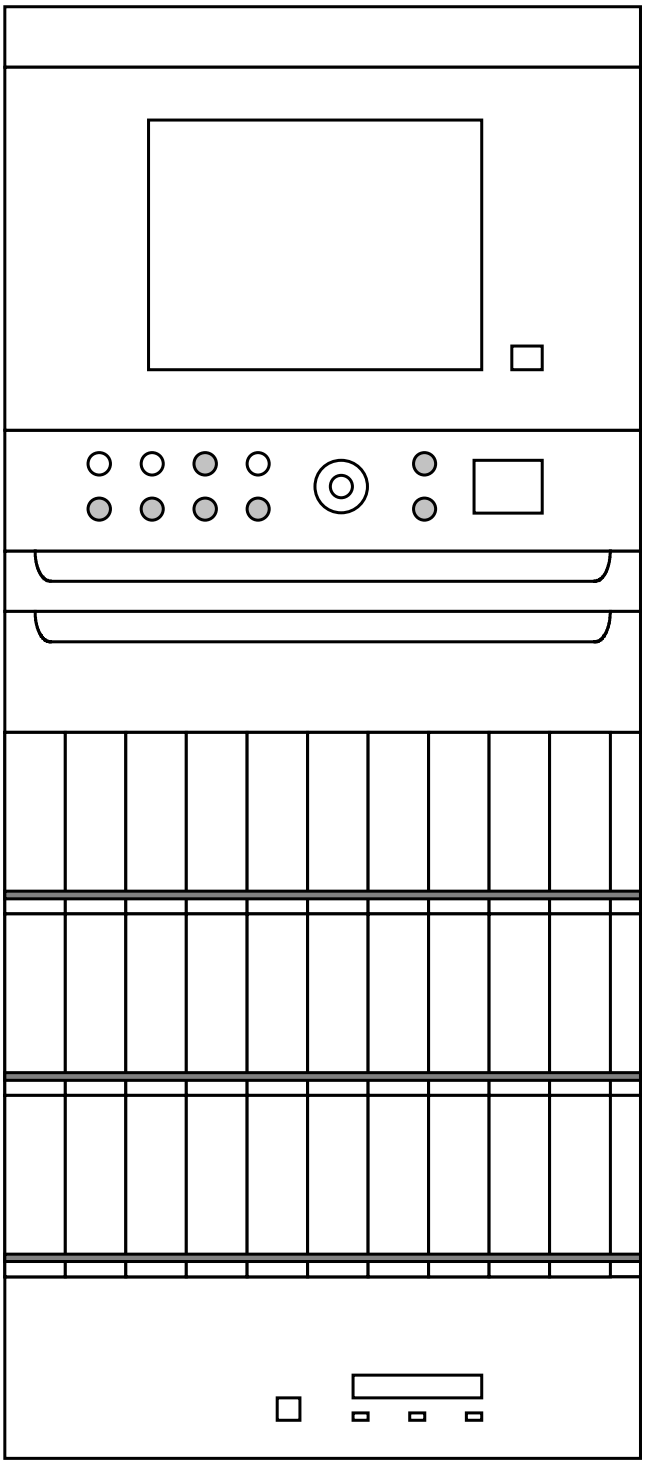

Figure 5-2: *Front view of RESECS measuring system*

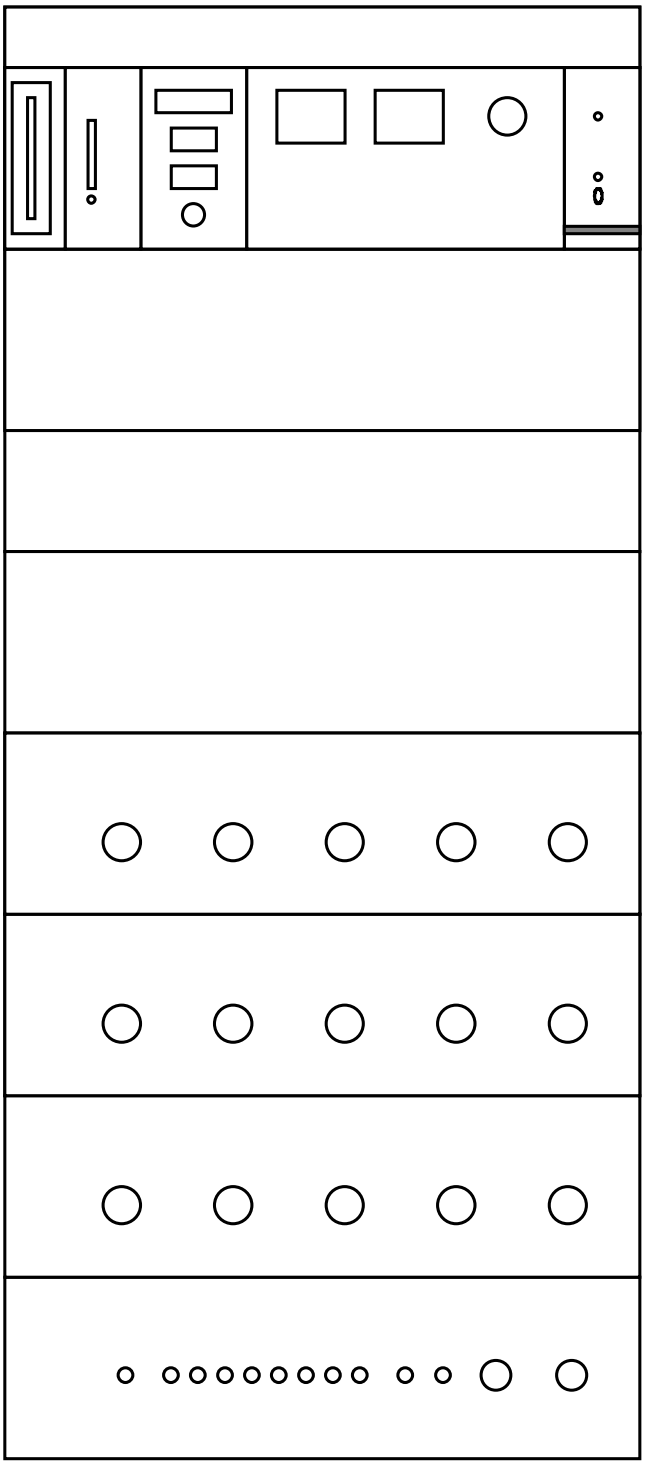

Measuring system chassis

Floppy disk
Secondary master HDD
LPT1, COM1, COM2, Ethernet
Control instruments: DC, AC input
Speaker
Cassette power rack

Connection panel 1

Decoder connection panel 1

Decoder group outlets:
000, 010, 020, 030, 040

Decoder connection panel 2

Decoder group outlets:
050, 060, 070, 080, 090

Decoder connection panel 3

Decoder group outlets:
0A0, 0B0, 0C0, 0D0, 0E0

Connection panel 2

Ethernet
External electrode outlets:
E00 - E07
P2C / Grounding
Enclosure ground
External emergency stop
AC input

Figure 5-3: *Rear view of RESECS measuring system*

The embedded PC (OCTAGON SYSTEMS PC510) is supplied with 33 MByte DRAM. The PC is set to the requirements of the measuring system. For detailed information refer to the PC510 users manual supplied on disk.

Further PC components are an ethernet card and two harddisk drives. The harddisks are formatted and partioned. The user has access to the secondary master harddisk. The secondary master harddisk may only be removed from the system when the system is turned off.

5.2.3 Injection Voltage Supply

The voltage supply, Xantrex XFR 600-2, serves as voltage supply for the injection current. This injection voltage source provides a maximum voltage of 600 V and a maximum current of 2 A. The voltage source is controlled by a serial PC interface (COM3). The switches on the rear panel of the voltage source are set to RESECS software requirements. For security reasons the output voltage is limited by software to 60 V in automatic monitoring measuring mode. In manual measuring mode the operator has full control over the output voltage.

5.2.4 Electrode Decoder Array

Electrode decoders are electronic circuits used for switching relays to the measuring lines C1, C2, P1 or P2. Each decoder has a unique address and four different functions. Decoders are supplied in groups of 16. They are denoted with hexadecimal numbers. The lowest digit defines the decoder number within a decoder group. The second digit defines the group number. The highest digit is reserved for internal use.

Example of DID´s (decoder identification)

000 - first decoder of first group

03A - tenth decoder of 4th group

0E1 - second decoder of 15th group

The system has a total number of 240 addressable electrode decoders.

The 18 pin electrode connectors at the rear panel of the system collect the outlets for one decoder group each. The decoders are connected to the pins in alphabetical order. They are denoted by the first decoder of the specified group. The pins labeled T and U are left unconnected.

Each 19" chassis contains 5 groups of decoders. A channel selector switch is located at the rear panel of the chassis. Remove the side cover of the enclosure to select the measuring channel for each group. As default setting, all groups are set to measuring channel 0. The hardware channel selection must be in accordance with software channel selection.

Activating and deactivating of electrode decoders is controlled by the measuring software. All decoders included in a measuring cycle are selected before the measurement and deselected before the next one. Only those decoders used for the next measuring cycle with the same function will not be deselected.

The supply voltage for the decoders is generated within the RESECS system.

It is galvanically isolated from other parts of the system. The decoder and relay supply current is displayed on the ampere-meter on the front of the system.

5.2.5 Uninterruptable Power Supply

The system is supplied with an uninterruptable power supply, Knuerr UPS Modul NP 2000c. The purpose of the UPS is to provide power to the entire measuring system for at least 60 minutes in the event of voltage breakdown or power failure. It is connected to the PC by a serial interface (COM2) and is able to monitor malfunctions of the supply voltage.

5.2.6 Measuring Procedure

The RESECS measuring software runs under MSWindows98. All input of measuring parameters is menu-driven. For detailed information refer to the RESECS software manual. The systems offers the possibility to create standard configurations like Wenner, Schlumberger, Dipole-Dipole as well as user defined configurations.

User defined configurations enable multi channel measurements. Up to six potential differences can be recorded simultaneously. These measurements require an user defined ASCII input file.

After creating a standard master project or an user defined master project all measurements can be controlled manually or automatically.

In monitoring mode the software creates copies of the master project and executes these daughter projects automatically. RESECS offers the opportunity to choose between different monitoring modi like start time controlled, interval controlled, number of cycle controlled or any combination of them. All measured values are stored on harddisk.

In the monitoring mode the voltage across the current electrodes is limited by software to 60V for security reasons.

A typical screen display of the measuring software is illustrated in figure 3. At the top of the screen the menu items and main control button bar are displayed. Furthermore the data window, a scope window, the pseudoarea plot and the pseudosection are activated.

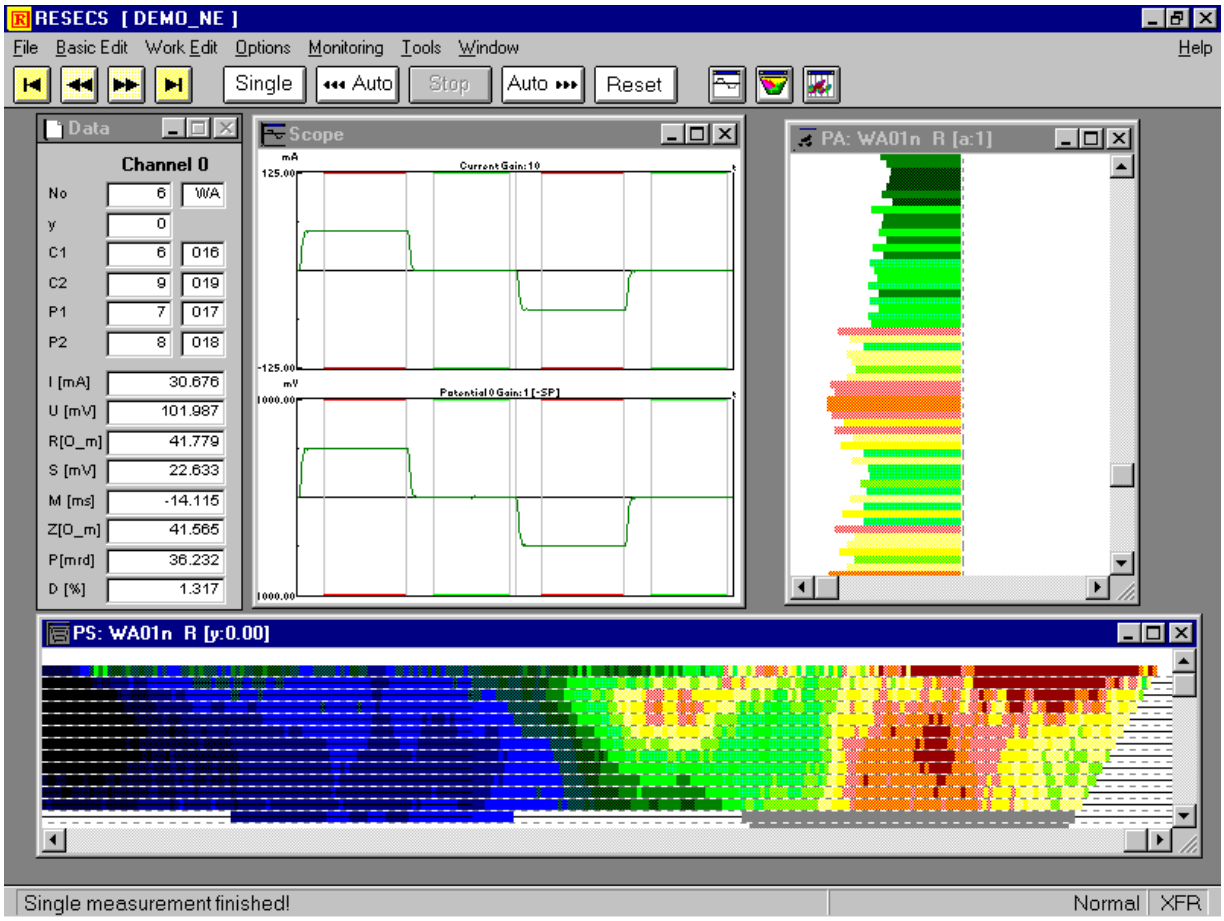

Figure 5-4: *Screen display of RESECS measuring software*

5.3 Instrumentation

Three areas will be instrumented in the Prototype Repository (Figure 5-5):

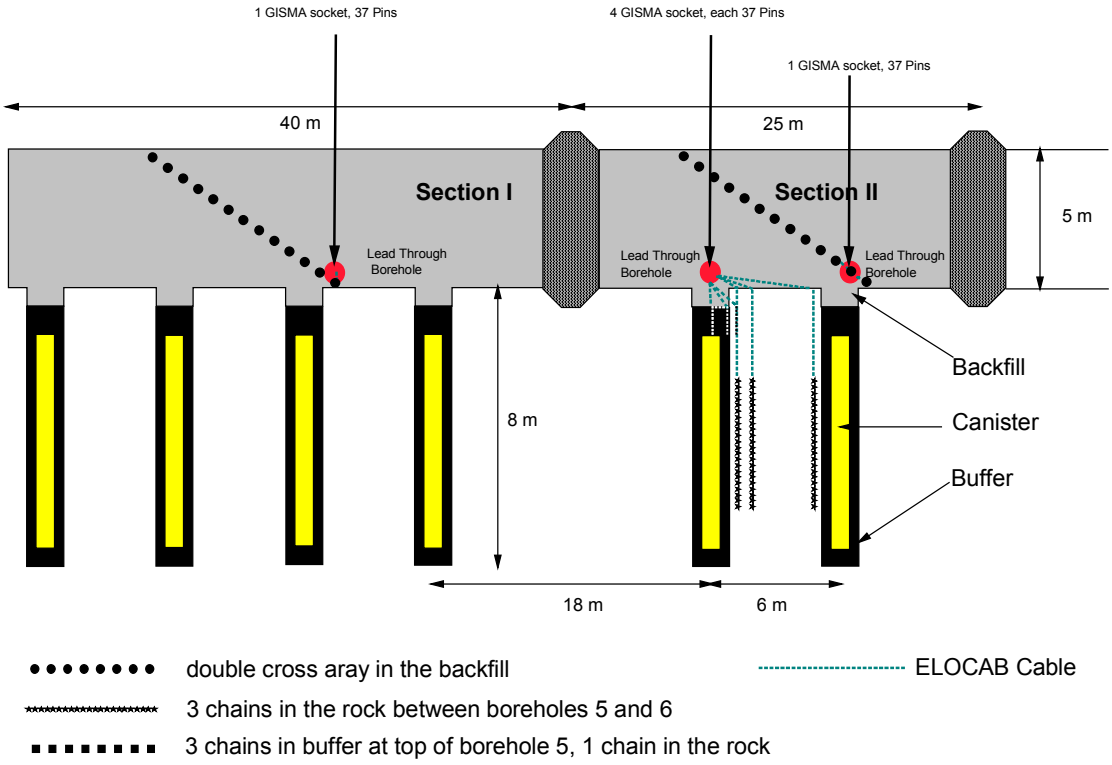

Figure 5-5: *Overview of electrode arrangements in the Prototype Repository*

5.3.1 Backfill

A double cross array (Figure 5-6) consisting of 36 single electrodes each with a spacing of 0.5 m will be installed on a 35° inclined backfill ramp above boreholes 2 and 3 in section I and above deposition boreholes 5 and 6 in section II. These arrays will monitor the resistivity distribution in the backfill.

5.3.2 Buffer

The resistivity in the buffer at top of deposition borehole 5 (Figure 5-7) will be determined by dipol-dipol measurements between one horizontal electrode chain being installed on the surface of the buffer and three vertical measuring chains being installed in the center of the buffer, about 10 cm from the borehole wall and outside of the borehole in the rock at 30 cm distance from the borehole wall. The spacing of electrodes will be 0.1 m The resistivity distribution will be determined in the plane enclosed by the buffer electrodes.

5.3.3 Rock

The resistivity distribution in the immediate vicinity of two of the deposition boreholes will be monitored with electrode chains being installed in three vertical boreholes in the rock between deposition boreholes 5 and 6 (Figure 5-5).

5.3.4 Electrodes and Electrode Chains

Differently sized electrodes will be manufactured for the different measurement arrays in the Prototype Repository. According to a recommendation of the Swedish Corrosion Institute the electrode material is a stainless steel type AISI 316 (also called SS2343).

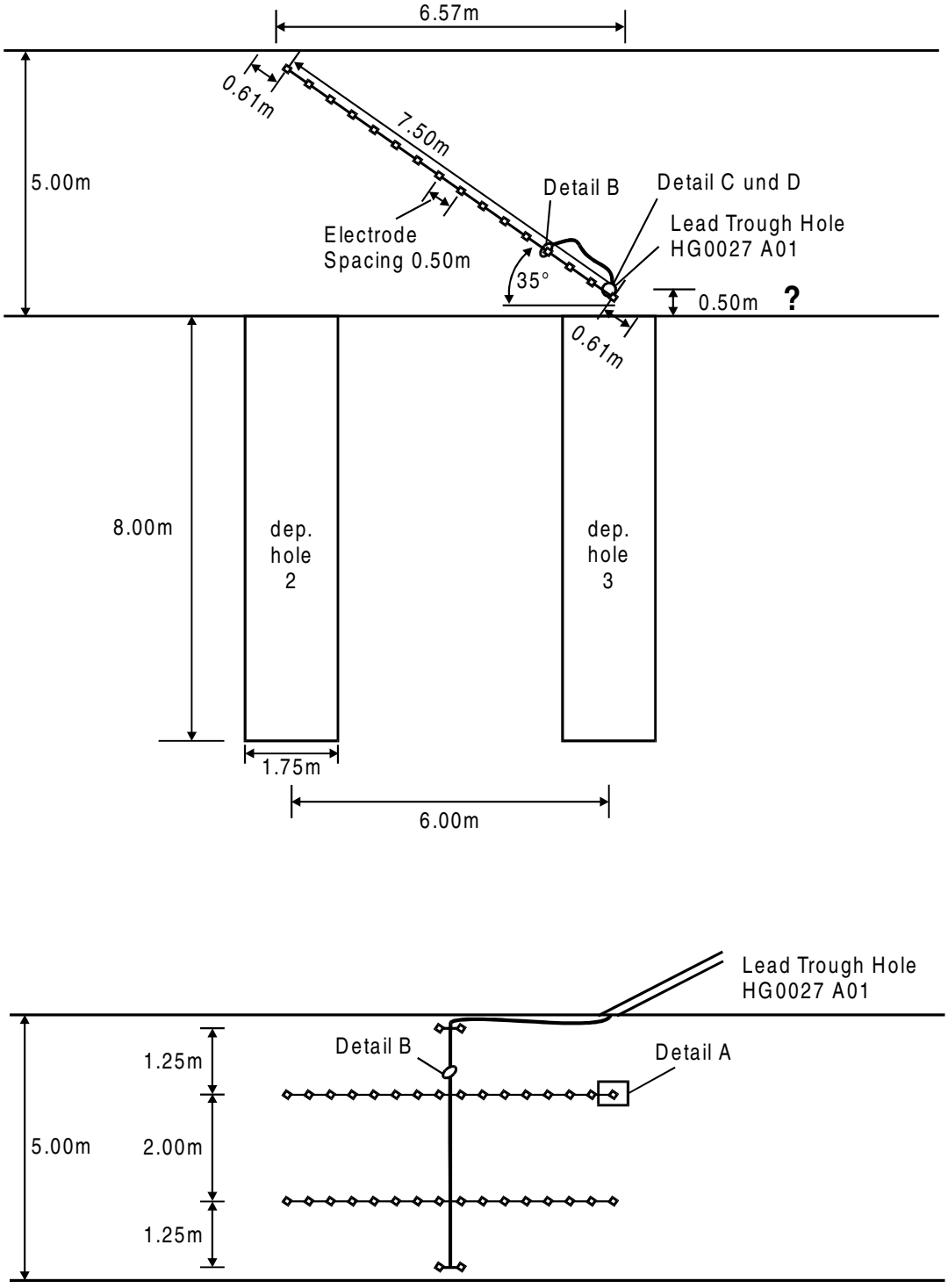

Figure 5-6: *Double cross electrode arrangement in the backfill*

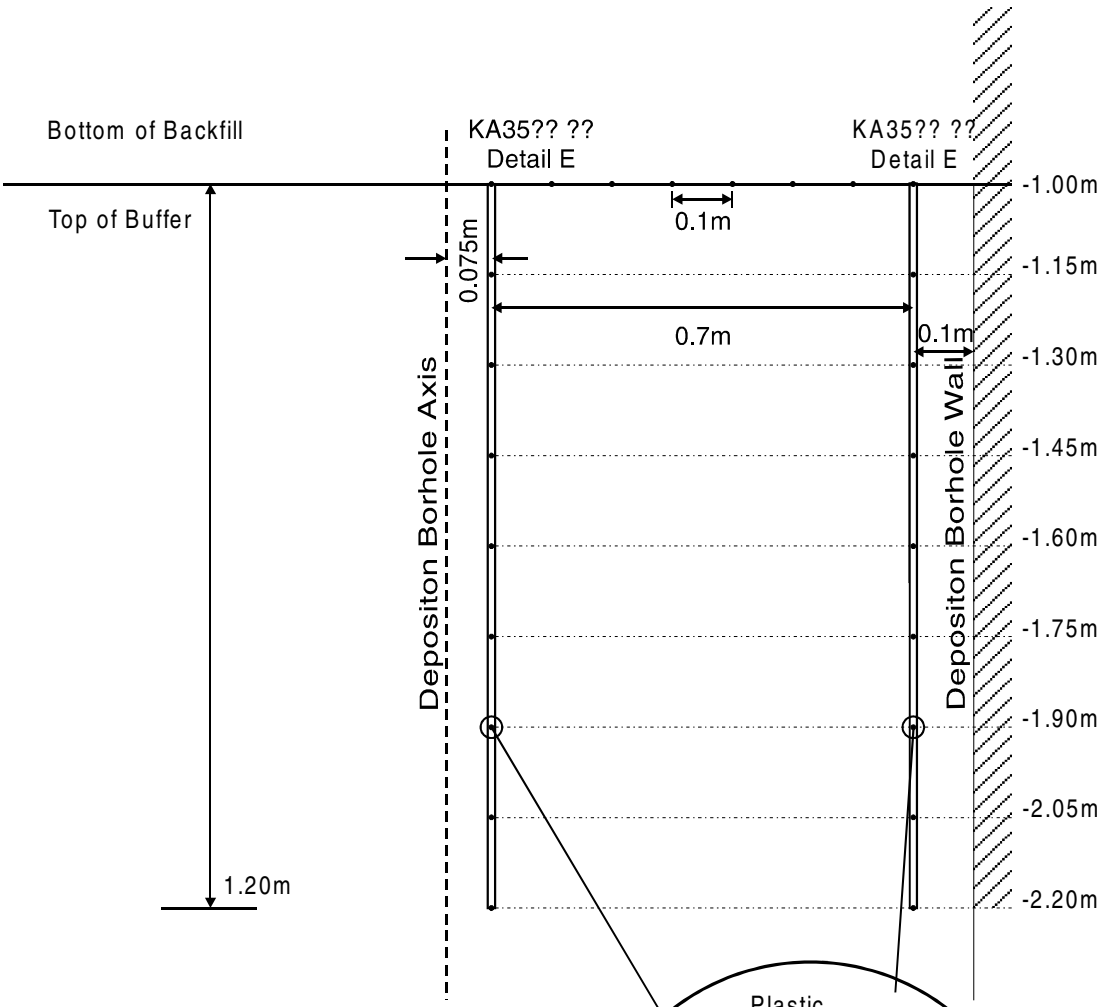

Specification	
Electrode:	10 x 10mm (round off)
Material:	X6CrNiMoTi17122 (1.4571, DIN 671 h9)
Wire:	1 x 0.75mm² (6 x 33 x 0.07mm)
Material:	Copper (Cu) tinned
Isolation:	Polyether-Polyurethan
Plastic Half Tube:	½ (2 x 40ø x 1000mm)
Material:	PVC (grey)
Sealing Compound:	
Material:	Silicon

ELECTRODE DETAIL E VERS.01.CDR

Figure 5-7: *Electrode chains at top of borehole 5*

The electrodes are manufactured according to Figure 5-9 with diameters of 10 and 30 mm, respectively with an accuracy of ± 0.1 mm.

Each electrode has a drillhole of 2 - 4 mm diameter and 5 – 10 mm depth in its neck in which the measuring wire will be fastened by silver soldering. The transition from the electrode to the cable is pasted with epoxy resin and sealed with a plastic sealing which is srewed onto the electrode's neck.

All electrode chains consist of an ELOCAB multiwire cable consisting of 37 insulated wires each filled with a swelling filler preventing migration of moisture inside the insulation sheathing (Figure 5-9). The cables are tight against a water pressure of 10 MPa perpendicular to the cable axis and 6 MPa along the cable axis.

The ELOCAB-cables are connected pressure tight to a GISMA-plug developed in submarine techniques (Figure 5-10). The GISMA-plugs are pressure tight, too up to water pressures of 10 MPa.

All electrode chains are of the same principle design shown in Figure 5-11. The multiwire part of the ELOCAB-cable reaches from the GISMA-plug to a seal from which onwards the single wires are cut to different lengths forming a chain. At each end of the single wire an electrode is fixed as described above.

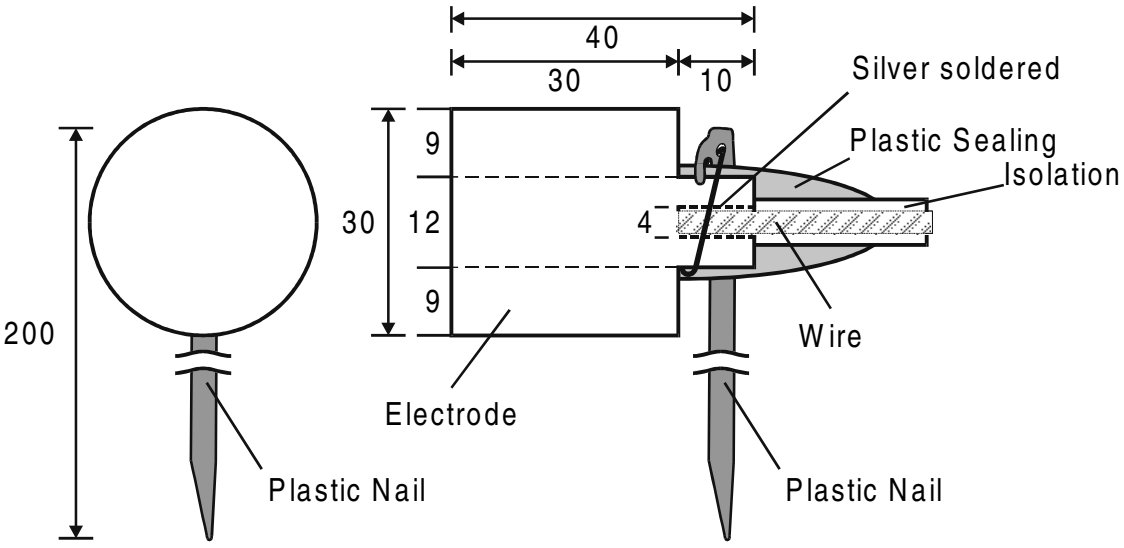

Figure 5-8: *Design of a drift electrode*

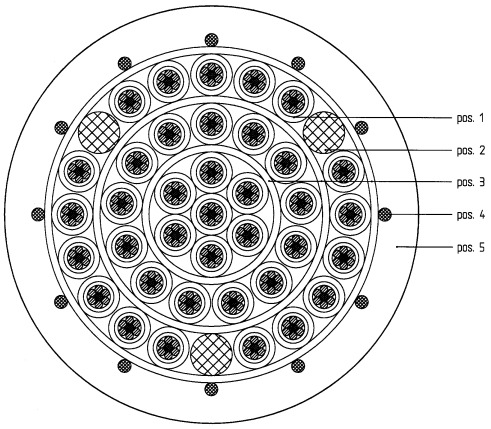

Figure 5-9: *Design of an ELOCAB-cable (diameter of multiwire cable: 27.5 mm, diameter of single wire: 2.7 mm)*

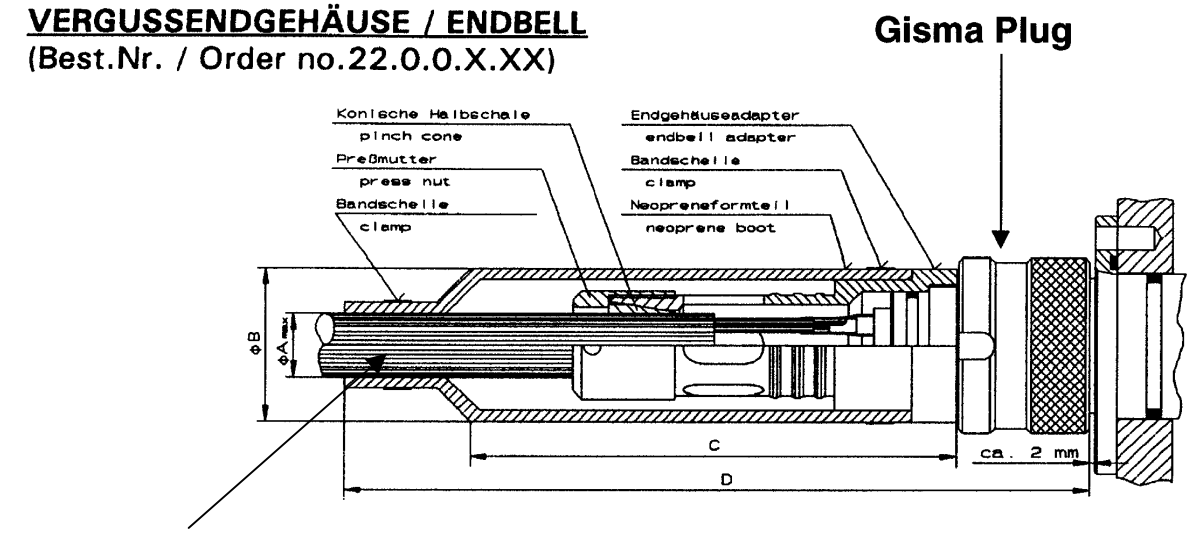

Figure 5-10: *GISMA-plug*

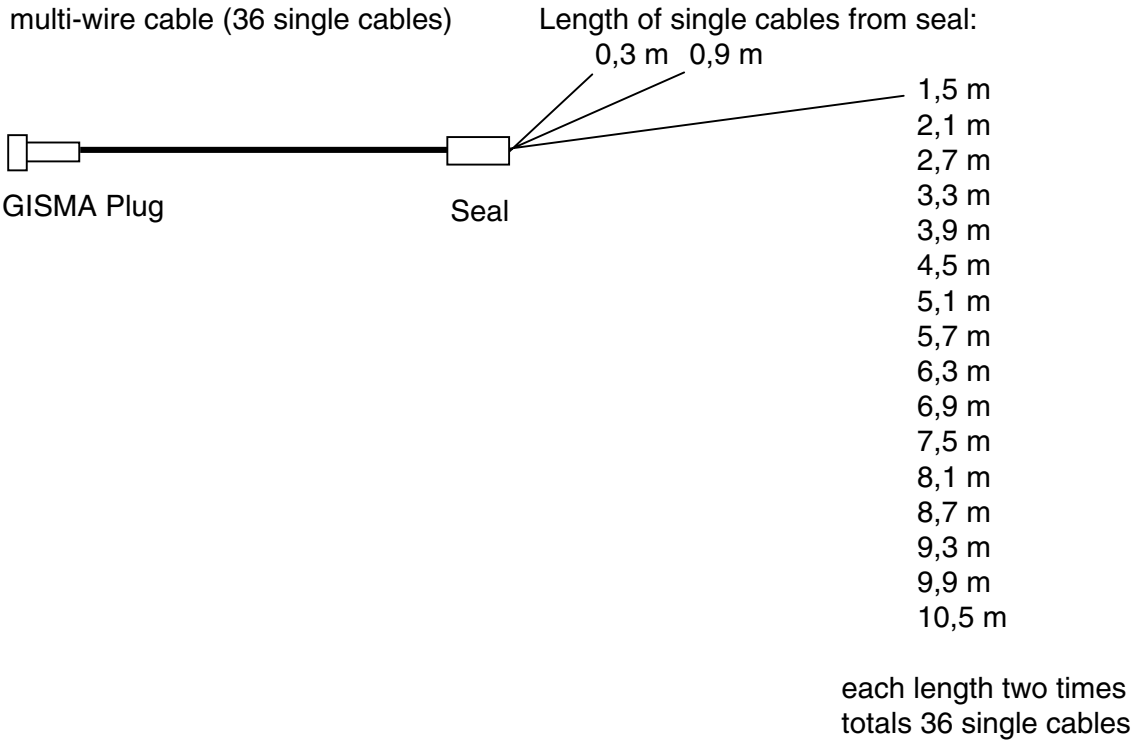

Figure 5-11: *Principle design of an electrode chain in the drift*

In the drift the chains consist simply of an ELOCAB-cable. The electrodes are fastened to the backfill by plastic nails. After installation of the chain, the GISMA-plug is plugged into a GISMA socket installed at the head flange of a lead-through hole in the drift wall.

The electrode chains in the buffer boreholes (Figure 5-12) consist of an ELOCAB cable with the single wires soldered to 10 mm electrodes which are fixed in the wall of a Plexiglas half tube. The single wires connected to the electrodes are sealed in the half tube with silicone and guided vertically upwards out of the buffer. The electrodes will be pressed against the buffer by filling the remaining volume of the borehole with bentonite powder produced during drilling of the borehole and compacting the bentonite as far as achievable to the design density of 1.66 g/cm^3 by stamping with a stick. Filling of the borehole and compaction of the buffer will be made in several steps with small portions of material in order to control the density of the compacted material over the whole borehole length. After installation in the buffer, the GISMA-plug of the cable is plugged into the respective GISMA socket in the drift wall.

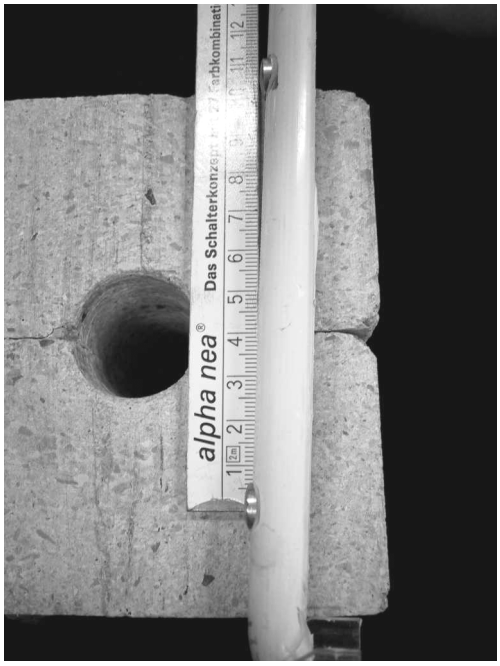

a) Test block of bentonite and
mock up electrode chain

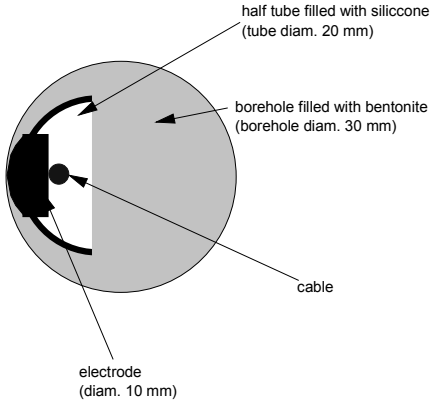

b) Horizontal cross section through buffer borehole

***Figure 5-12**: Design of electrode chain in the buffer*

The electrode chains in the rock (Figure 5-13) consist also of an ELOCAB cable with the single wires soldered to 10 mm electrodes which are fixed to a plastic stick which is lowered into the borehole in the rock. To get proper contact of the electrodes to the rock the boreholes are grouted with a special cement/crushed rock mixture. After installation in the borehole, the GISMA-plug of the cable is plugged into the respective GISMA socket in the drift wall.

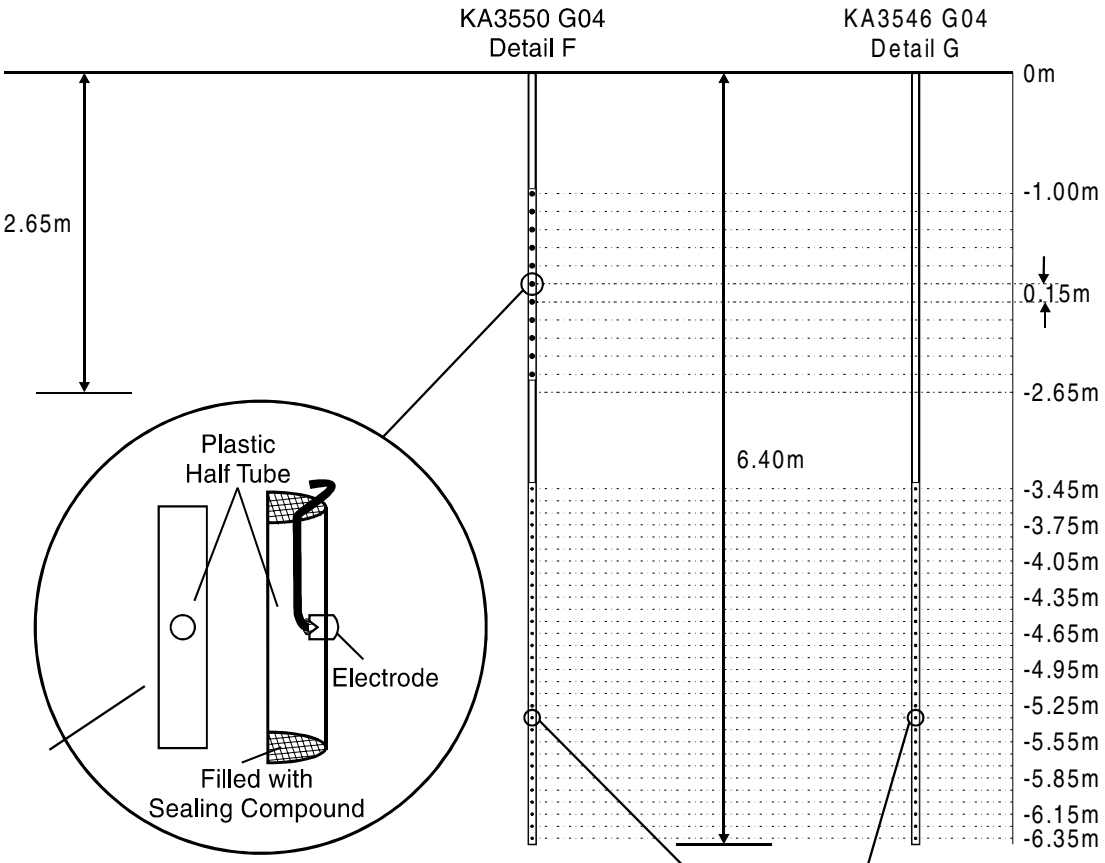

Specification	
Electrode:	10 x 10mm (Detail F/G)
Material:	X6CrNiMoTi17122 (1.4571, DIN 671 h9)
Wire:	1 x 0.75mm² (6 x 33 x 0.07mm)
Material:	Copper (Cu) tinned
Isolation:	Polyether-Polyurethan
Plastc Stick:	5 x 20 x 3000 (Detail F/G)
	Material: PVC (grau)
Sealing Compound:	
Material:	Epoxy Resin or Silicon

Figure 5-13: *Design of electrode chain in the rock*

6 Laboratory Calibration

In order to enable adequate interpretation of the in-situ measurements, calibrations were performed at GRS's geotechnical laboratory in Braunschweig.

The calibrations include the determination of the resistivity of compacted MX-80 powder and of original pre-compacted buffer material samples provided by SKB as well as of the drift backfill in dependence of the water content and of temperature.

Besides its dependence on the water content, the electrical resistivity is also a function of salinity and composition of the pore solution. Since both may change as the solution penetrates the buffer and the backfill, investigations were performed in order to quantify this effect.

6.1 Resistivity of MX-80-Bentonite

6.1.1 Samples

6.1.1.1 Preparation of compacted MX-80 samples with defined water content

For the preparation of the samples with different water contents, the MX-80 powder was moisturized with ÄSPÖ-solution as presented in see Table 6-1.

Table 6-1: Composition of the used ÄSPÖ-solution [mmol/l]

Na	K	Ca	Mg	Cl	SO_4
79.67	0.25	17.06	3.33	113.92	3.40

After drying of the MX-80 powder in an oven at 105 °C over 24 h, the water content of the delivered MX-80 material was determined to 9.8 wt %. Under consideration of this value, the total water content of the samples was obtained by adding an adequate amount of Äspö solution.

Subsequently, the moist powder was compacted in a specially constructed resistivity measurement cell (see Figure 6-1) to a dry density of 1.66 g/cm3 which is considered a representative value for the conditions at the top of a deposition borehole (Dahlström 1998). For each water content a new sample was produced. The specifications of prepared samples and their water content are shown in Table 6-2.

Table 6-2: Water content and size of the prepared MX-80 samples and of the original buffer samples

sample	water content	sample length	sample diameter
	wt %	mm	mm
compacted MX-80 samples			
MX-80/1	11	100.0	40
MX-80/2	16	100.0	40
MX-80/3	22	96.1	40
MX-80/3a	22	95.0	40
MX-80/4	27	86.4	40
MX-80/5	33	87.1	40
samples from original ÄSPÖ buffer material			
ÄSPÖ-PR-BFST 13/1	13	97	50
ÄSPÖ-PR-BFST 13/2	12	97	50
ÄSPÖ-PR-BFST 13/3	12	97	50
ÄSPÖ-PR-BFST 17/1	14	97	50
ÄSPÖ-PR-BFST 17/2	14	97	50
ÄSPÖ-PR-BFST 17/3	14	91	50

6.1.1.2 Preparation of original ÄSPÖ MX-80 buffer samples

Cylindrical samples were prepared from original bentonite bricks provided by SKB. These samples had a different initial water content of about 13 and 17 wt%, respectively. Three samples were prepared from the 13-wt%-material and marked as ÄSPÖ-PR-BFST 13/1 to 13/3 and three further samples from the 17-wt%-material marked as ÄSPÖ-PR-BFST 17/1 to 17/3.

The water content of the original bricks was determined on material remaining from sample preparation by drying in an oven at 105 °C over 24 h.

The size of the samples and their water content at time of investigation are summarized in Table 6-2.

6.1.2 Measurement and Evaluation

The resistivities of the compacted MX-80 samples with varying water content were measured at ambient temperature in the specially constructed cell shown in Figure 6-1. At the ends of a Plexiglass tube, the current electrodes A and B were installed. Since the samples varied in length, the electrode B was moveable. Two brass rings (voltage electrodes M and N) were inserted in the Plexiglass tube.

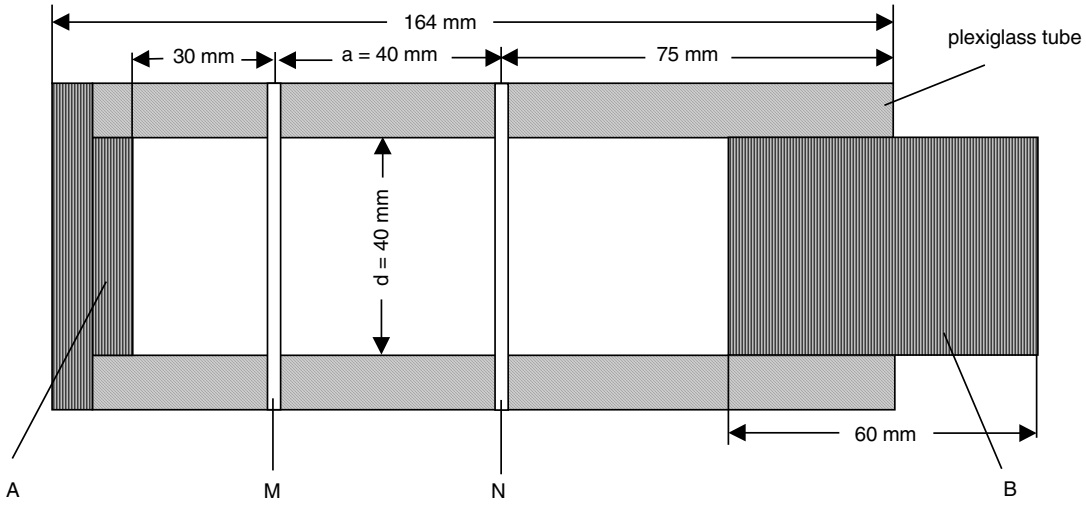

Figure 6-1: *Schematic view of the resistivity measurement cell for compacted MX-80 samples*

For the resistivity measurement of the samples prepared from the original bricks, the cylindrical samples were set between two metal plates A and B (Figure 6-2). A potential difference U was measured at the electrodes M and N which had been installed at the surface of the sample.

The resistivity of the samples was determined by using the four-point method. The current I was conducted at the current electrodes A and B of both sides of the sample and the difference in the electrical potentials U was measured at the voltage electrodes M and N. According to (Schick et al. 1973) and (Kull et al. 2001), the resistivity was calculated by:

$$\rho = \frac{U \cdot A}{I \cdot a} \qquad (18)$$

with:

ρ = resistivity [Ωm]

U = electrical voltage [V]

I = current [A]

a = distance of the voltage electrodes M and N

A = surface area of the sample [m^2]

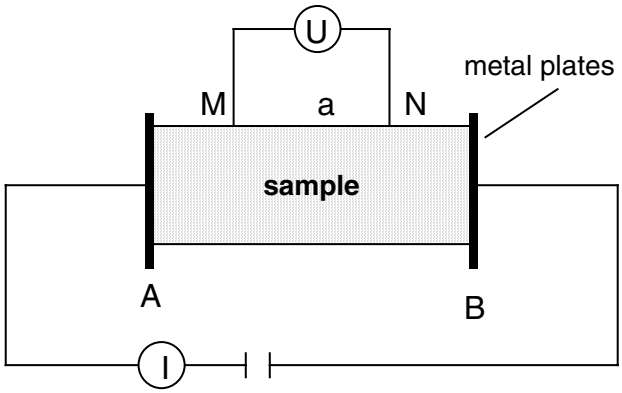

Figure 6-2: *Schematic experiment layout for the determination of sample resistivity*

6.1.3 Results

The results show that the resistivities of the compacted MX-80 samples decrease with increasing water content (Figure 6-3). The resistivities range between 34.5 and 1.6 □m. The water content varies between 11 and 33 wt %. The highest resistivity (34.5 □m) was measured at the lowest water content of 11 wt %. A small increase of the water content to 16 wt % already leads to a significant decrease of resistivity (6.8 □m). At higher water contents above 22 wt % up to 33 wt %, the change of resistivity is insignificant.

The resistivities of the original buffer material range between 6.3 □m and 7.8 □m at water contents of about 12 and 13 wt % (samples ÄSPÖ-PR-BFST 13/1 to 13/3) and 3.8 □m and 4.5 □m at water contents of about 14 wt % (samples ÄSPÖ-PR-BFST 17/1 to 17/3). The resistivities are in the same range as those of the compacted MX-80 samples at comparable water contents. The water content and the corresponding resistivities are summarized in Table 6-3.

The steep drop of resistivity at the lower water contents can be explained by a clay-typical interface conductivity which is due to additional cations held loosely in the diffuse part of the electrical double layer surrounding the clay particles (Serra 1984). Already a small amount of solution leads to formation of a double layer and causes the interface conductivity.

Because of the relatively small resistivity changes observed at higher saturation it seems obvious that the interface conductivity is the predominant part of the conductivity in the MX-80 bentonite.

The total conductivity is a sum of the conductivity of the free solution in the pore space and the interface conductivity. According to Schopper (1982), the conductivity of a solution saturated porous rock can be described by

$$\sigma_0 = \frac{1}{F}\sigma_w + \sigma_{q0} \qquad (19)$$

with σ_0 being the total conductivity of the fully saturated rock, F the formation factor, σ_w the electrolytic solution conductivity, and σ_{q0} the interface conductivity.

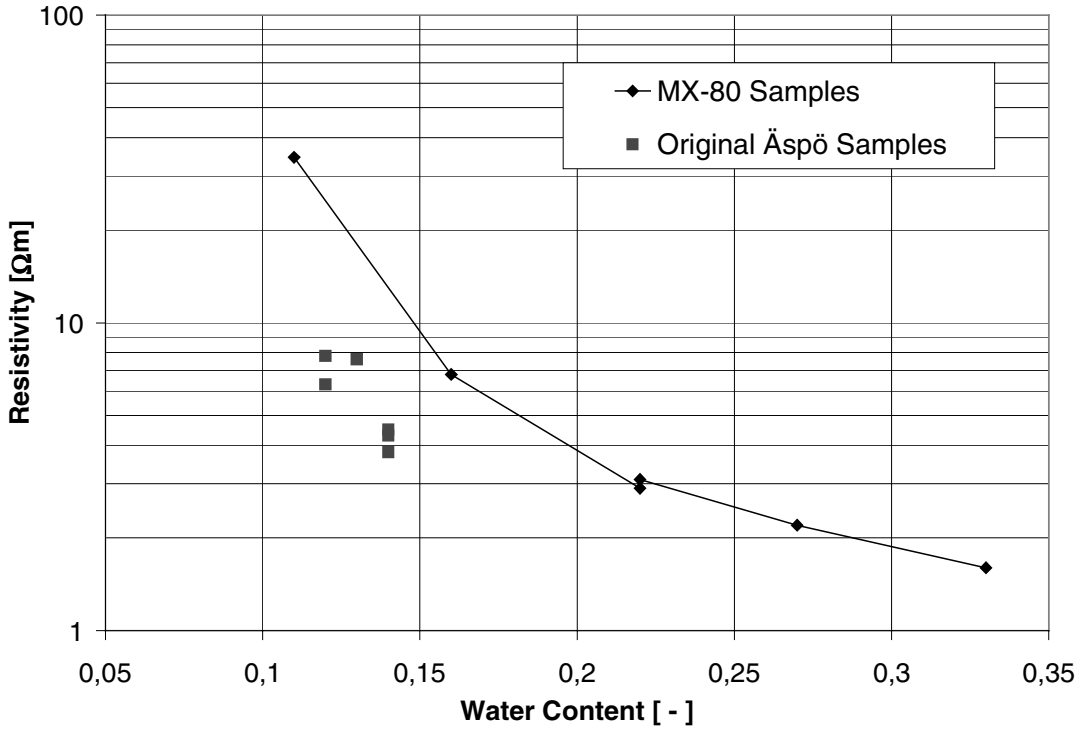

Figure 6-3: *Resistivity of compacted MX-80 samples and original ÄSPÖ buffer material as a function of the water content*

Table 6-3: Summary of the water content and the resistivities of the compacted MX-80 samples and the original ÄSPÖ buffer material

MX-80 sample	water content	resistivity
	wt %	Ωm
compacted MX-80 samples		
MX-80/1	11	34.5
MX-80/2	16	6.8
MX-80/3	22	2.9
MX-80/3a	22	3.1
MX-80/4	27	2.2
MX-80/5	33	1.6
samples from original ÄSPÖ buffer material		
ÄSPÖ-PR-BFST 13/1	13	7.6
ÄSPÖ-PR-BFST 13/2	12	6.3
ÄSPÖ-PR-BFST 13/3	12	7.8
ÄSPÖ-PR-BFST 17/1	14	3.8
ÄSPÖ-PR-BFST 17/2	14	4.5
ÄSPÖ-PR-BFST 17/3	14	4.3

6.2 Drift Backfill

6.2.1 Samples

For reasons of comparison, the backfill samples were prepared to represent the backfill conditions right after installation. These are the design density of 1.7 g/cm3 and the initial water content of 12 wt% which means a dry density of the backfill of 1.5 g/cm3.

The initial water content of both the crushed rock and the Milos bentonite were determined according to DIN 18121-1 by drying in an oven over 90 hours at 105 °C and subsequent measurement of the weight loss. According to the measurements, the crushed rock has an initial water content of 1.20 wt% and the Milos bentonite of 13.09 wt%.

Samples of differently moisturized backfill were prepared by first mixing pure crushed rock and Milos bentonite as delivered by SKB and subsequent spraying of predetermined amounts of Äspö water (compare Table 6-1) into the material until the desired total water content was achieved. Seven samples as shown in Table 6-4 were prepared.

Table 6-4: Water content and achieved dry density of backfill samples

Backfill sample	Water content	achieved dry density
	wt%	g/cm^3
Sample 1	12	1.33
Sample 2	13	1.53
Sample 3	15	1.45
Sample 4	18	1.48
Sample 5	21	1.50
Sample 6	25	1.51
Sample 7	33	1.27

Figure 6-4 shows emplacement of the moisturized material into the specially designed and fabricated measurement cell and Figure 6-5 shows a four-point-measurement set-up. All samples were manually compacted as far as possible to achieve the dry density of 1.5 g/cm3. Especially at the highest water content of 33 wt% it was impossible to achieve the dry density of 1.5 g/cm3 because the material was very sticky. Regarding the determination of electrical conductivity or resistivity, however, all samples were considered acceptable.

6.2.2 Results

For different water contents, the resistivity measurements of the compacted crushed rock/Milos bentonite samples were performed at 22 °C and 35 °C. The results are presented in Figure 4-6. Both resistivity curves show a decrease in resistivity with increasing water content. The resistivities measured at 22 °C range between 16.3 Ωm and 1.9 Ωm at water contents of 12 wt% and 33 wt%. The resistivities measured at 35 °C are lower and show values between 9.7 Ωm and 1.7 Ωm at comparable water contents. These results are in good

Figure 6-4: *Emplacement of moisturized backfill into measurement cell for determination of material resistivity*

Figure 6-5: *Measurement set-up for determination of backfill resistivity*

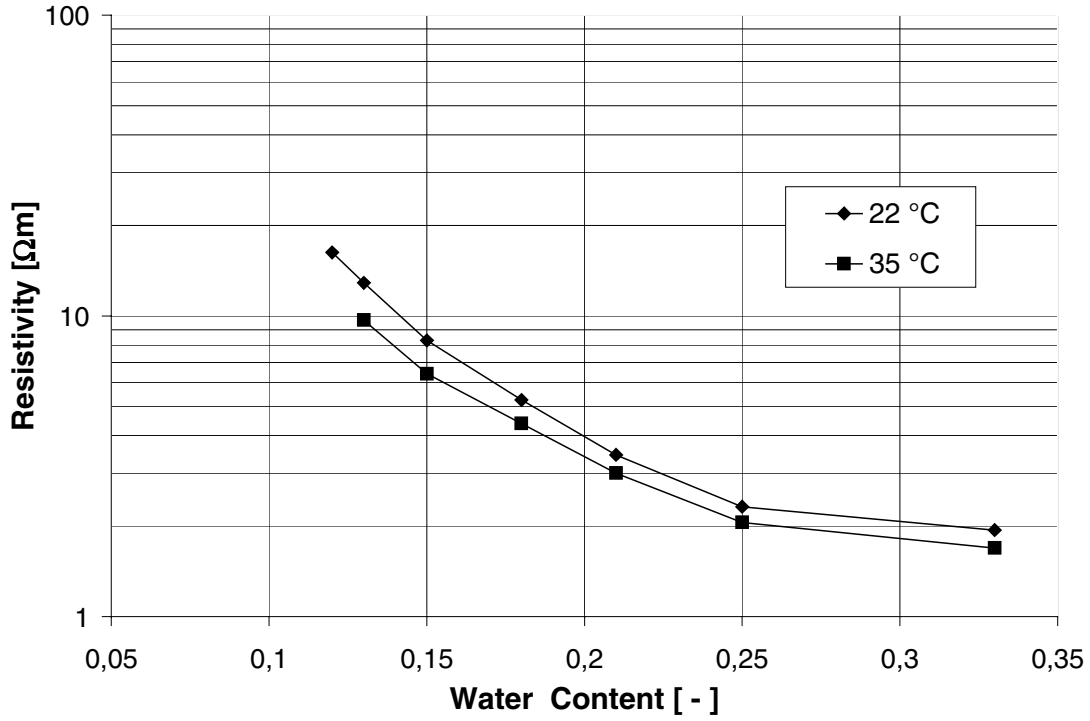

Figure 6-6: *Resistivity of compacted backfill samples versus water content*

agreement with the results obtained on compacted MX-80 samples and original ÄSPÖ MX-80 buffer samples and show the same characteristic steep resistivity decrease at lower water contents. Because of the similar behaviour of buffer and backfill it is concluded in addition, that the bentonite governs the resistivity behaviour of the backfill.

The resistivities at the higher temperature (35 °C) are lower than the values measured at 22 °C. This is explained by the temperature dependence of the pore solution, because the conductivity of most electrolyte solutions increases with increasing temperature. But it can be caused by the temperature influence of the resistivity of the bentonite or the rock material, too. For a better interpretation, appropriate investigations would be necessary.

Rock

Regarding the granitic rock, calibration results are available from earlier laboratory measurements (Zimmer 2001). Six samples of Äspö granite from the ZEDEX drift were saturated with original formation water. For a full saturation of the granite which implies a water content of app. 0.5 Vol.-%, a resistivity of 1000 Ωm was measured. Afterwards, the samples were dried to decrease the water content. Due to the lower water content, the resistivity increased. The results are shown in Figure 6-7.

The electric resistivity of the samples was measured as shown in Figure 6-2 by applying a known voltage to the planes of the sample and measuring the resulting current. To achieve a good coupling between the metal plates and the sample, the planes of the sample were coated by highly conductive silver paint. The three samples which were measured with silver-coated planes show less scattering of the values compared to the samples without a silver-coating.

In case of rocks with constant porosity, the relation between resistivity and water content is described by Archie's law (equation 20). In this equation, ρ is the total resistivity of the rock, ρw the resistivity of the water, Φ the porosity, S the saturation, m the so called cementation factor, and n the saturation exponent. With this law, the determined values can be fitted by an exponential curve and the constants in Archie's law can be specified.

$$\rho = \rho_w \cdot (\Phi \cdot S)^{-m} \qquad (20a)$$

$$\rho = \rho_w \cdot \Phi^{-m} \cdot S^{-n} \qquad (20b)$$

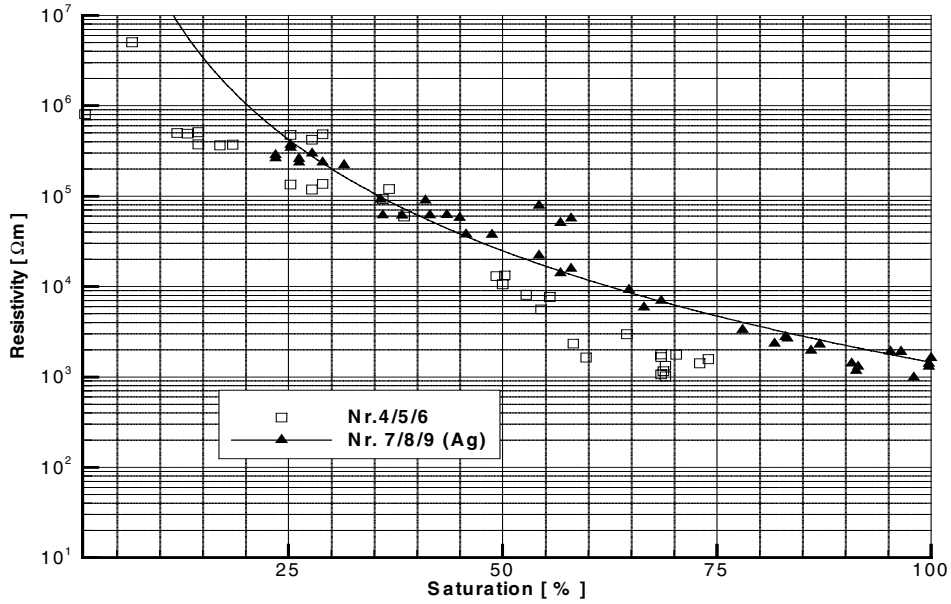

Figure 6-7: *Correlation between resistivity and saturation on granite samples from HRL Äspö*

6.3 Change of Composition of Äspö-Solution by Interaction with Compacted MX-80

These experimental investigations intend to give information about the change of composition which Äspö solution might experience on its way through compacted MX-80. For the situation given in a deposition borehole filled with blocks of compacted bentonite it seemed possible that infiltrating solution changes composition not only due to cation exchange processes. It is the micro structure of the built-in material which induces additional effects. Ultrafiltration of solution (the separation of dissolved salts and water) must not be excluded a priori. The phenomenon of ultrafiltration with compacted clays has been described and investigated extensively elsewhere, e. g., (Hanshaw et al. 1973), (Kharaka et al. 1973), (Kharaka et al. 1976), (Demir (a) 1988), (Demir (b) 1988), (Dresner et al. 1963), (Kemper et al. 1964), (Marshall 1948), (Kemper et al. 1963), (Benzel et al. 1984), (Ishiguro et al. 1996). Within the context of this report

it is important to note that compaction density, sample height, particle size (or even size of pellets), and method of compaction may have an impact on the course of percolate composition during an experiment. Further, the rate of flow has an impact on the efficiency of ultrafiltration.

For the reasons given, data gained by batch experiments with suspended clay don't give reliable information on the change of solution during infiltration. As the electrical conductivity of aqueous solution depends on mass and composition of its solutes, the change in electrical conductivity for the system compacted bentonite – salt – water may change while the actual water content remains the same. To quantify the possible impact of change in solution composition on the electrical conductivity of partially saturated bentonite it is necessary to know the change of solute composition as Äspö solution protrudes into the clay barrier.

6.3.1 Materials and Methods

The experiment being conducted is done with a cell normally taken for the determination of swelling pressures. The bottom frit of the pressure cell was covered with filter paper to prevent it from clogging. 16.1 g MX-80 representatively probed were placed on it and treated with a spatula to produce an approximately horizontal surface. Compaction proceeded with ca. 1 MPa/min (with sample radius of 2.5 cm, this gives 1901 N/min) to a sample height of 0.51 cm giving a dry density of 1.66.

Compaction pressure was held constant for 15 min to ensure de-airation of the sample. Then the sample was allowed to relax by deloading it. After 1 min, the sample was compacted again to the desired height and the load held constant for again 15 min. This procedure was repeated until no relaxation occured anymore and thereby a sample was obtained consolidated at a dry density of 1.66 g/cm3. The uncertainty of dry density was ± 0.01 g/cm3.

The piston was fixed with the screw cap on top. This way, the exact geometry of the sample is known throughout the experiment.

The general set up of the experiment is shown in Figure 6-8.

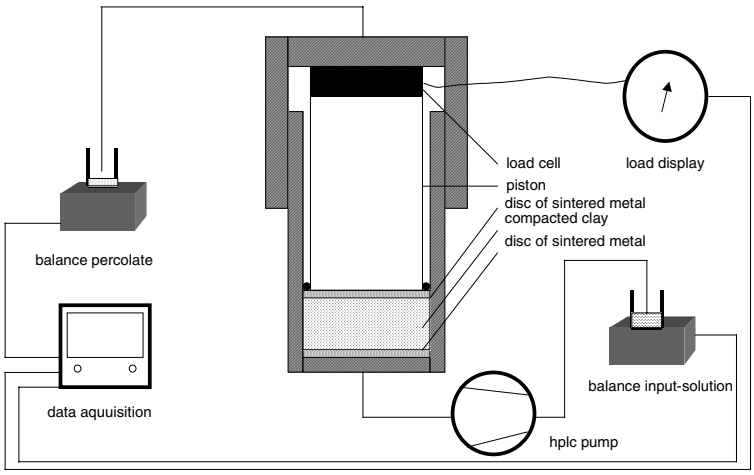

Figure 6-8: *Experimental set-up of percolation experiment*

The gas-filled headspace of containments for both inflowing and outflowing solution were connected via capillary tubes with small bottles of Äspö solution to prevent evaporation during the experiment. Containments for outflowing solution were changed at intervals ranging between 1 and 4 days. By appropriate weighing an exact mass balance was maintained for inflowing and outflowing solution, and hence for the percolated bentonite.

The HPLC-pump delivers the solution at a constant rate of 0.0020 ± 0.0003 ml/min up to a maximum fluid pressure of 47 bar. This corresponds to the maximum likely hydrostatic pressure in the Äspö URL. Also the pump rate compares well with the maximum seepage rate given by SKB. The experiment is run under ambient temperature conditions, which by dayly measurement is given with 22.1 ± 0.7°C.

The discontinuously taken percolates are characterized by the measurement of their density and concentrations of Na, K, Mg, Ca, and SO4. Concentration of chloride is calculated by difference.

Table 6-5: Planning data for percolation experiment

Diameter of sample:	r =	2.46	[cm]
	h =	0.51	[cm]
Volume of sample:	V =	9.7	[cm^3]
Grain density of MX-80:	ρ_G =	2.439	[g/cm^3]
Target density:	ρ_{Target} =	1.66	[g/cm^3]
Necessary mass of MX-80:	m_{Clay} =	16.1	[g]
CEC:	CEC =	0.73	[mol_c/kg]
CEC of sample:	CEC_{Sample} =	0.01175	[mol_c]
Grain volume of sample:	V_G =	6.6	[cm^3]
Remaining pore volume:	V_P =	3.1	[cm^3]
Normality of Äspö solution:	$N_{Solution}$ =	120.58	[$mmol_c/l$]
Charges in 1 pore volume Äspö solution:	q_{VP} =	0.00037	[mol_c]
Necessary pore volumens for 1 x CEC_{Sample}:	n_{VP} =	31.5	[1]
... corresponding to	V_{CEC} =	97.4	[cm^3]
Powder density of MX-80:	ρ_{bed} =	1.034	[g/cm^3]
Bed depth:	h_{bed} =	0.82	[cm]
Target rate of flow:	J_{normed} =	1	[cm^3/cm^2*d]
Cross sectional area of sample:	A =	19.0	[cm^2]
Total rate of flow:	J =	19.0	[cm^3/d]
... corresponding to	J =	0.79	[cm^3/h]
... corresponding to	J =	0.013	[cm^3/min]

The composition of inflowing "Äspö solution" was calculated as the mean of 55 single sets of analytical data as delivered by SKB. Minor solute components were neglected. With a small correction for electroneutrality, the composition given in Table 6-1 was obtained. Figure 6-9 gives an overview of the variation of probed Äspö solution with sampling date.

6.3.2 Results

Criteria for the termination of the experiment were initially planned to be constant values for

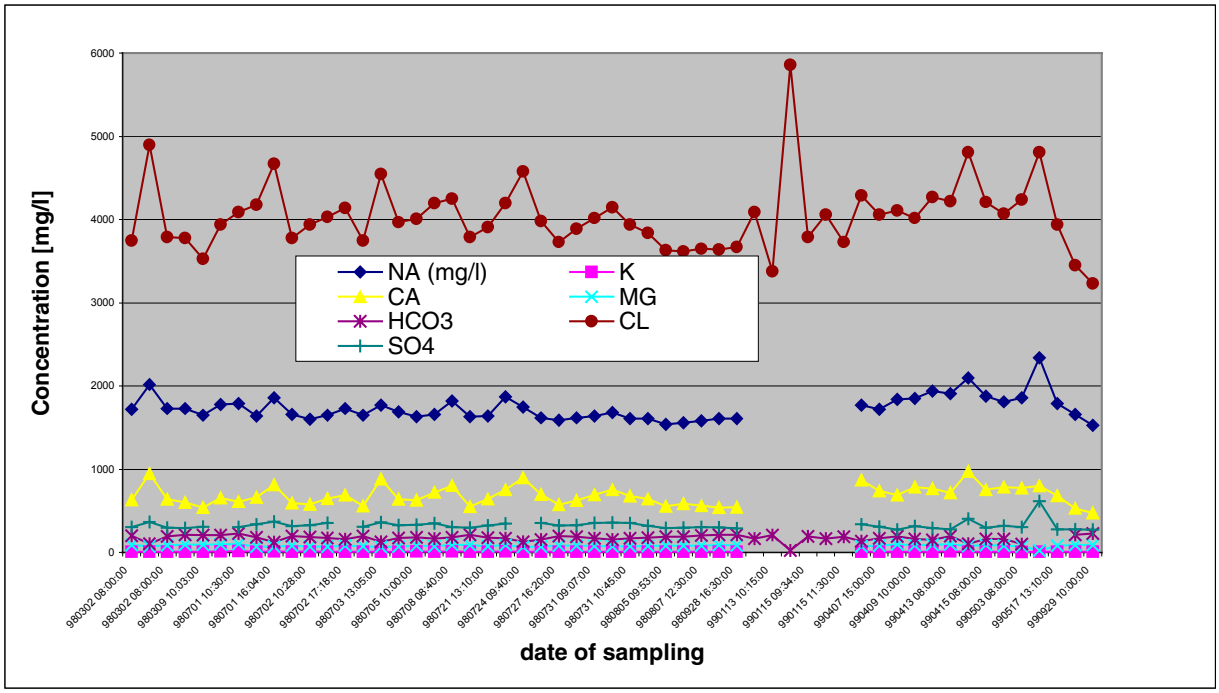

Figure 6-9: *Composition of Äspö solution. All concentrations in mg/l.*

outflowing solution density and –composition (which should be the same like the one of inflowing Äspö solution). However, at the time of this report a condition of equilibrium between Äspö solution and sample is not established yet.

The change in solution composition is depicted in Figure 6-11 to Figure 6-16. All measured concentrations were related to the total mass of percolated solution. This is not exactly, but quite the mass of water percolated. The first data point in all cases represents the inflowing Äspö solution. Its value is marked by a horizontal "baseline" in each figure. In general, it may be concluded that at the beginning of the experiment the sample takes up Mg and Ca from solution while Na and K are being released. The second data point (which represents the first solution having left the sample) indicates dissolution of some minor components of MX-80. As the normality of percolate remains to be higher than that of Äspö-solution, this process seemingly remains to continue during the whole experiment. It cannot be explained with cation exchange. This becomes obvious when the normality of the percolate is regarded (Figure 6-10). It is defined as

$$N = c_{Na} + c_K + 2 \cdot (c_{Mg} + c_{Ca}) \quad (21)$$

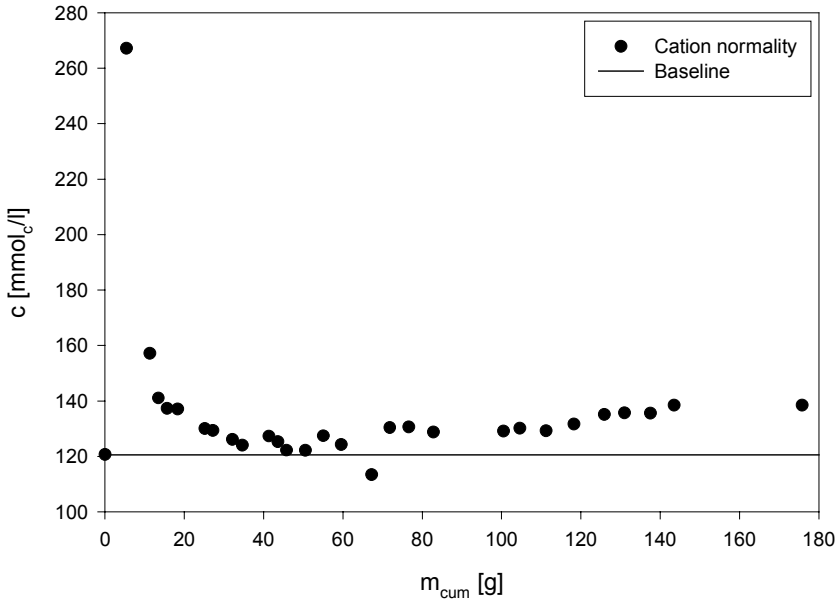

Figure 6-10: *Change of normality of percolate. Note that normality is constantly a bit higher than that of inflowing solution.*

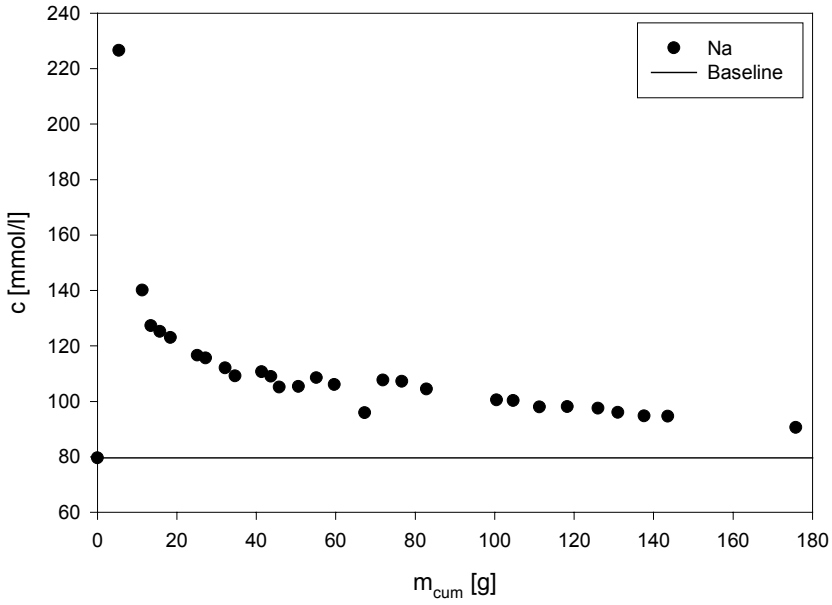

Figure 6-11: *Na-concentration in Äspö-solution after penetrating compacted MX-80*

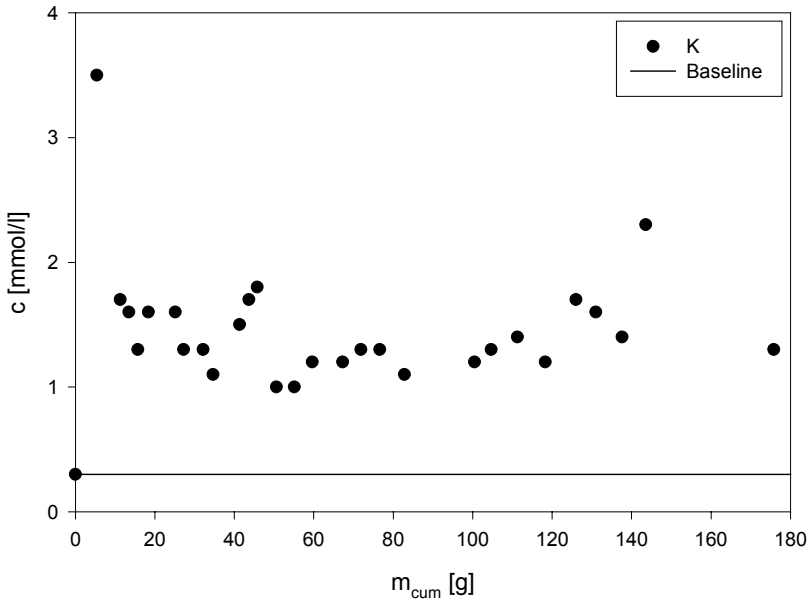

Figure 6-12: *K-concentration in Äspö-solution after penetrating compacted MX-80*

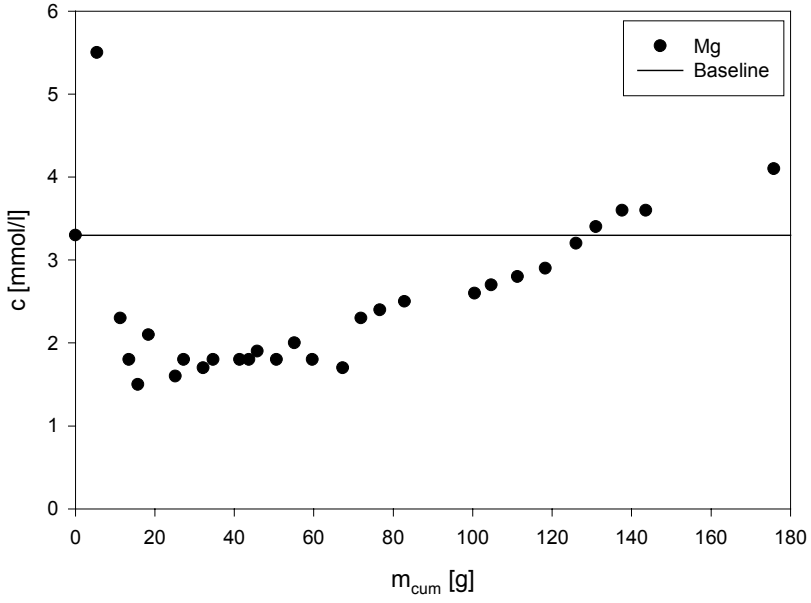

Figure 6-13: *Mg-concentration in Äspö-solution after penetrating compacted MX-80*

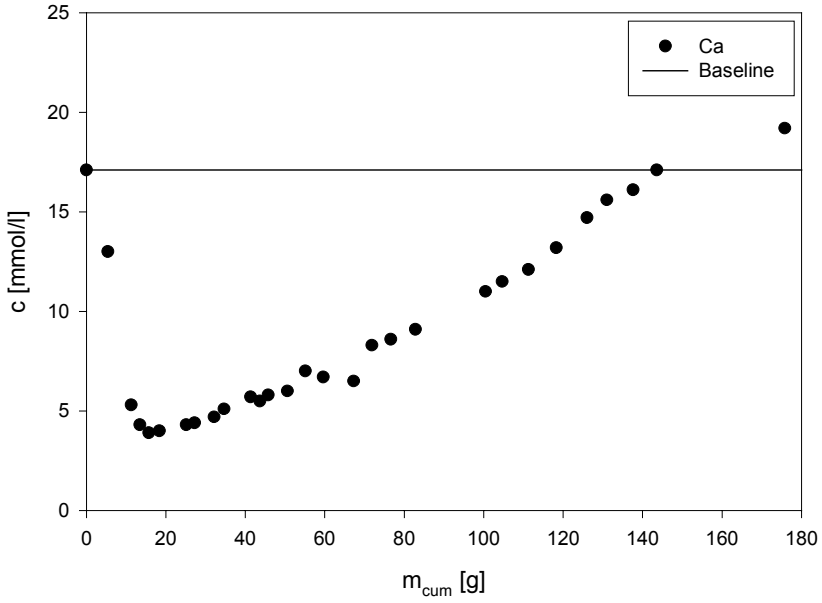

Figure 6-14: *Ca-concentration in Äspö-solution after penetrating compacted MX-80*

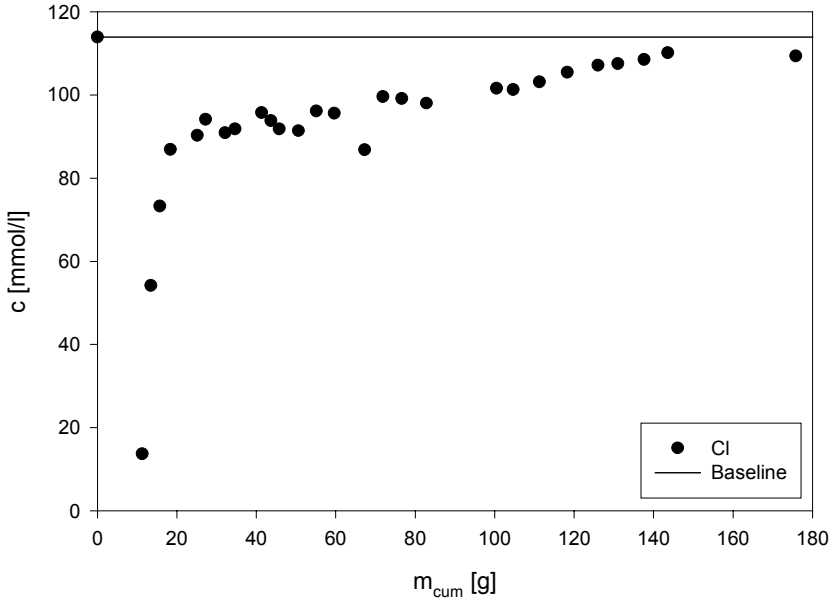

Figure 6-15: *Cl-concentration in Äspö-solution after penetrating compacted MX-80*

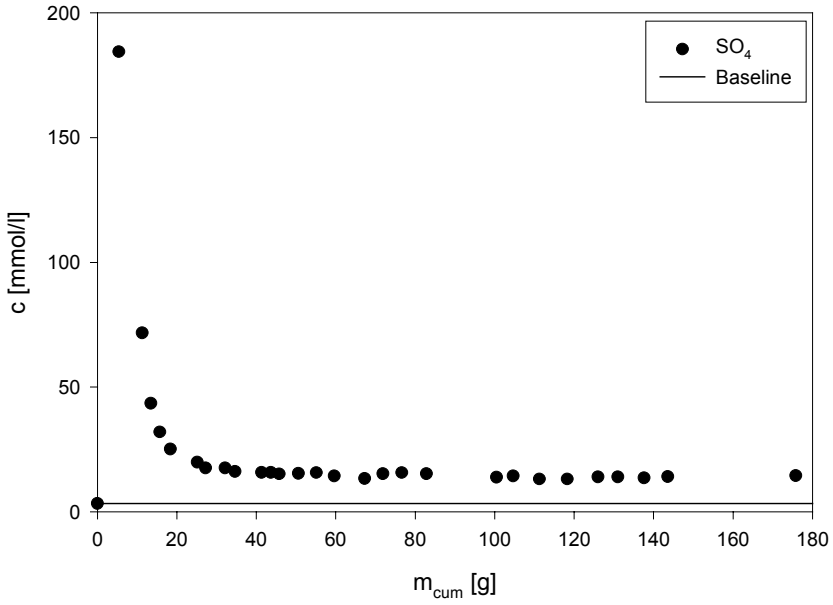

Figure 6-16: *SO_4-concentration in Äspö-solution after penetrating compacted MX-80*

With the first solution entering the clay, salt is mobilized which adds to the total salinity introduced by the Äspö solution. On the grounds of purely cation exchange reasoning, also the increase in sulfate would not be expected. This might be due to the oxidation of pyrite present in the material. The content of chloride was calculated from the charge difference of the cations (Na, K, Mg, Ca) and sulfate.

Figure 6-15 shows that the content of chloride in the very first volume increments is replaced in favour of sulfate. At the present state of the experiment, chloride concentration is still lower than that of the inflowing solution, while in the contrary, sulphate continues to be mobilized from the sample.

From the salt content in the percolate, the compacted MX-80 under the given conditions of salinity, flow rate, and compaction density does not seem to behave like a semipermeable membrane. After an initial increase in salinity, the overall salt content in terms of normality comes very close to but is not exactly like the one of the inflowing solution.

Generally, three processes can possibly occur within the sample: cation exchange, mineral dissolution, and ultrafiltration.

Cation exchange. At low ionic strengths this reaction proceeds charge-neutrally. That means that for any charge transferred into the adsorber phase a same charge is exchanged into the solution phase. Due to the formation of chloro complexes with alkaline earth metals, this law seemingly is not fullfilled. What is the extent of chloro complex building in Äspö-solution? Taken the stability constant for CaCl+ at 298.15 K and 1 atm pressure (Johnson 1979) (Johnson 1981):

$$\log K_{CaCl^+} = 0{,}42 \qquad (22)$$

This is in a certain proportion to the conditional stability constant (Sposito 1989):

$$\log K_{CaCl^+} = \log^c K_{CaCl^+} + 0{,}512\left[\frac{\sqrt{I}}{1+\sqrt{I}} - 0{,}3I\right]\Delta Z^2 \qquad (23)$$

with

$$\Delta Z^2 \equiv \upsilon_c m^2 + \gamma + \upsilon_a I^2 - (\upsilon_c m + \gamma - \upsilon_a I)^2 \qquad (24)$$

In the preceding equation, the valences of any constituent building up the complex with the general formula $M^{m+}_{\upsilon_c} H^{+}_{\gamma} L^{I-}_{\upsilon_a}$ are accounted for. With the ionic strength pertinent for Äspö-solution, equations 22 and 23 give after rearrangement:

$$\frac{[CaCl^+]}{Ca^{2+}} = 10^{0{,}18}[Cl^-] \qquad (25)$$

Equation 25 may be solved iteratively to give a set of mutually consistent sets of constituent-concentrations, logcKCaCl+ and ionic strength. For the present purpose it might be sufficient to make an estimate by introducing the pertinent chloride concentration in Äspö-solution. The result is that about 17% of calcium (and presumeably Mg) is present as monovalent chloro complex, giving rise to (seemingly) non-electroneutral cation exchange. Practically, this means for the present case that by the adsorption of Ca and Mg (as CaCl+ and MgCl+, respectively) cation normality in solution decreases.

The observed change of composition of percolate indicates that Mg and Ca are adsorbed in favour of Na and K. It is hypothesized that both cations are at least partially adsorbed in the form of their chloro complexes. This is in accordance with the systematically "too low" concentration of chloride as compared with its input concentration. On the other hand, chloride is not likely to be removed from solution by precipitation, because geochemical calculation does not indicate saturation of any chloride-bearing mineral phase (see below).

In the last increments of percolate, however, Mg and Ca begin to be released from the sample. Thus, the overall trend of cation concentrations seems to indicate that the dominating process at the end of experiment is mineral dissolution rather than cation exchange.

Mineral dissolution. MX-80 bentonite contains a number of accessory minerals, e. g., calcite and pyrite. These minerals are likely to dissolve upon contact with Äspö-solution. Mineral dissolution will tend to enhance salinity of solution, i. e., cation and anion normality.

The observed change of composition with respect to sulfate indicates that mineral dissolution happens to some degree, because sulfate is not involved in cation exchange. Geochemical modelling (EQ36) indicates no saturation whatsoever (Figure 6-17). However, this information must be regarded with caution, because within the limited range of laboratory work funded and due to the small volumes of percolate taken at each increment, no carbonate contents could be

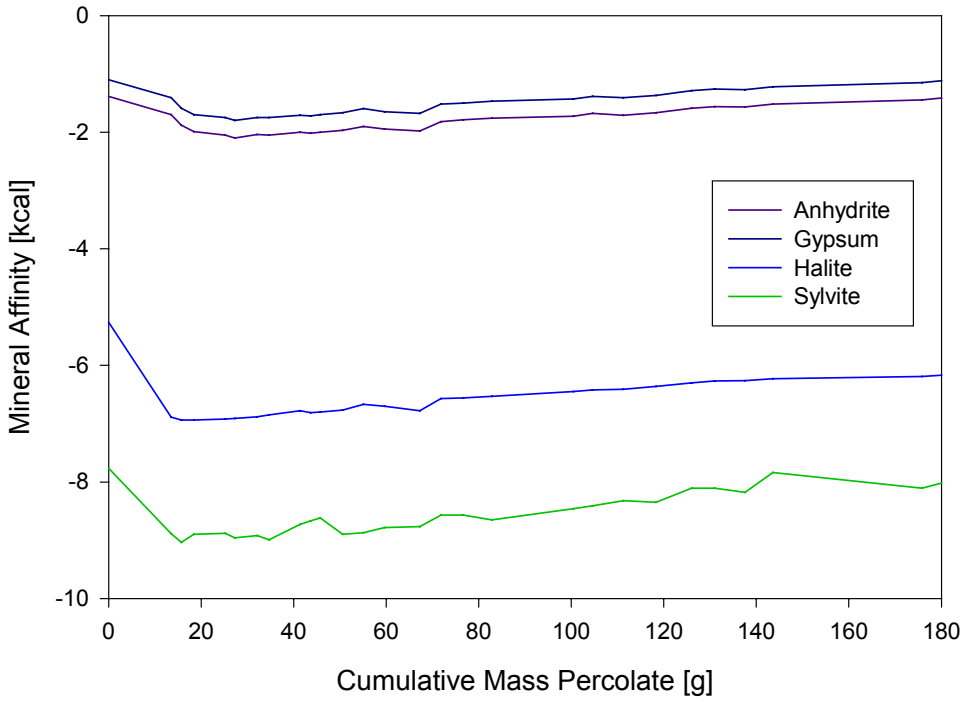

Figure 6-17: *Mineral saturation states in percolates*

determined. As MX-80 contains appreciable amounts of calcite it might well be possible that the percolate contains small amounts of carbonate adding to the charge balance constraint which served as base of calculation for chloride content.

Ultrafiltration. As mentioned above, compacted clays may behave like semipermeable membranes, retaining salt and rendering the percolating solution to a lower salinity. This effect would have a considerable impact on the electrical conductivity of the solution. However, the obtained data do not indicate any ultrafiltration to occur under the conditions applied.

Letting aside ultrafiltration, cation exchange and mineral dissolution will occur simultaneously within the sample. Ultimately, percolating solution should exhibit the same composition like the inflowing solution. Since this is not the case, either of both processes has not come to an end. We consider mineral dissolution as being the rate controlling process with cation exchange equilibrium establishing itself accordingly. The almost linear course of sulfate indicates a state of stationary equilibrium where some accessory mineral (perhaps pyrite) dissolve.

Approximately 30 pore volumes have penetrated the sample which is about one surface charge in terms of dissolved cations. The mass of penetrated solution exceeds the six-fold of the mass of bentonite.

This experiment was initiated by the "fear" that compacted bentonite could act as semipermeable membrane. By the retention of salt, electrical conductivity would have been significantly diminished. The results show that under the given conditions of solution composition, flow velocity, compaction density, layer thickness, temperature and bentonite composition no salt retention is observed. The overall salinity of solution, however, is higher than that of Äspö-solution, which we suppose to be the consequence of mineral dissolution. Whether this leads to a changing electrical conductivity of solution depends on the partial molar conductivity of each species present and needs to be measured in artificial solutions.

7 Assessment of Measurement Resolution

Modelling has been performed on basis of the laboratory calibration results to assess the measurement resolution which can be expected from the in-situ measurements and to support the design of the electrode arrays.

The laboratory calibrations have shown that the buffer and backfill material will already have a rather small resistivity around 7 Ωm and 16 Ωm, respectively, when installed (at a water content of 12 to 13 wt.%). In conjunction with the comparably high resistivity of the rock (approx. 1000 Ωm at full saturation), this may have the effect that resistivity reductions by increasing water uptake in the buffer and backfill cannot be properly detected if all electrodes for the buffer measurements are located in the rock or the electrodes in the backfill are located too close to rock. In order to clear this issue, model calculations have been performed to determine optimum electrode arrangements, enabling high resistivity resolution.

Modelling was performed by calculating the expected measurement values for a given set of measurement configurations. Afterwards, the artificial measurement values were evaluated by inverse modelling (compare chapter 3.2).

7.1 Backfill

Results of geoelectric modelling of the prototype repository drift using an elliptic drift model were not sufficient with an electrode configuration around the drift surface. The presence of the surrounding high-resistive rock seemed to cause a high-resistivity "ghost" anomaly in the drift center. In order to clear up whether this result is due to insufficiencies of the employed computer code or whether it is inherent to the model and electrode configuration, two simplified rectangular models were investigated.

In both models, the drift has a rectangular cross section, and the electrodes (36 in total) are located along the drift surface. In the first model, there is no surrounding rock, that means the backfilled drift is isolated. In the second model, a highly resistive rock (1000 □m) surrounds the drift. The drift itself consists of a lower "wet" backfilled part (2 □m) and an upper "dry" backfilled part (16 □m). Modelling was performed by calculating artificial measurement results from the input model and afterwards performing an inversion of the "measured" data.

Figure 5-1 shows the first input model (left) and the corresponding inversion result (right). Obviously, the input model is well reconstructed by the inversion algorithm. The resolution is satisfying.

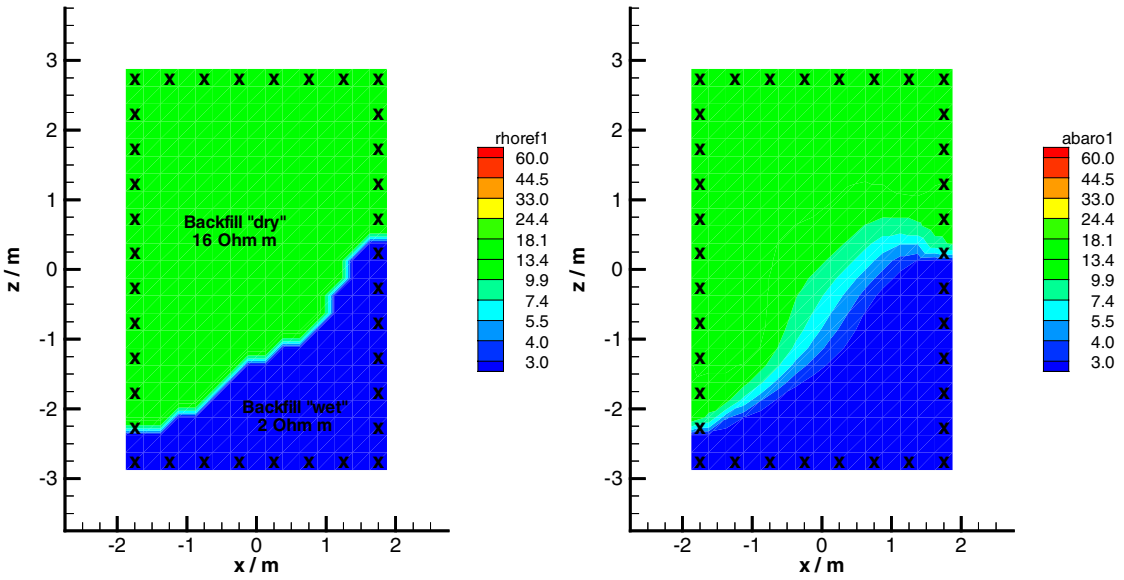

Figure 7-1: *Geoelectric modelling of the prototype repository backfill: Rectangular model without surrounding rock (left: input model, right: inversion result)*

The second input model (with rock) and the corresponding inversion result are shown in Figure 7-3. Here, the high-resistivity ghost in the drift center appears again. That means the ghost does not result from an disadvantageous geometry in the original elliptic drift model, but is created as soon as the highly resistive rock is included in the model. Placing all the electrodes on the border between rock and drift will, in any case, cause this problem. Since the rock is there in reality, it cannot be left out in the model. Therefore, the only solution is an altered electrode configuration. Modelling with the elliptic drift model and different electrode configurations have shown that adequate results can be expected if a double cross of electrodes as shown in Figure 7-3 is being installed. The "measured" resistivity change is reconstructed sufficiently in this case.

7.2 Buffer

Various models were investigated in order to determine the most adequate electrode arrangement for the buffer. The first model used the originally planned arrangement of four electrode chains located outside the buffer in the rock. This led to completely insufficient results for the buffer. Further modelling included an additional electrode chain centered in the buffer or a chain placed horizontally on the buffer surface. While the horizontal chain gave only little improvement, the additional central chain led to better results when the buffer was modelled as homogeneous dry (7 □m) or homogeneous wet (4 □m). For the most interesting case, however, which incorporates a partially wetted buffer, again no satisfying results could be achieved. The modelling results with the original model, the model with an additional central electrode chain, and with a horizontal chain are shown in Figure 7-4 to Figure 7-6.

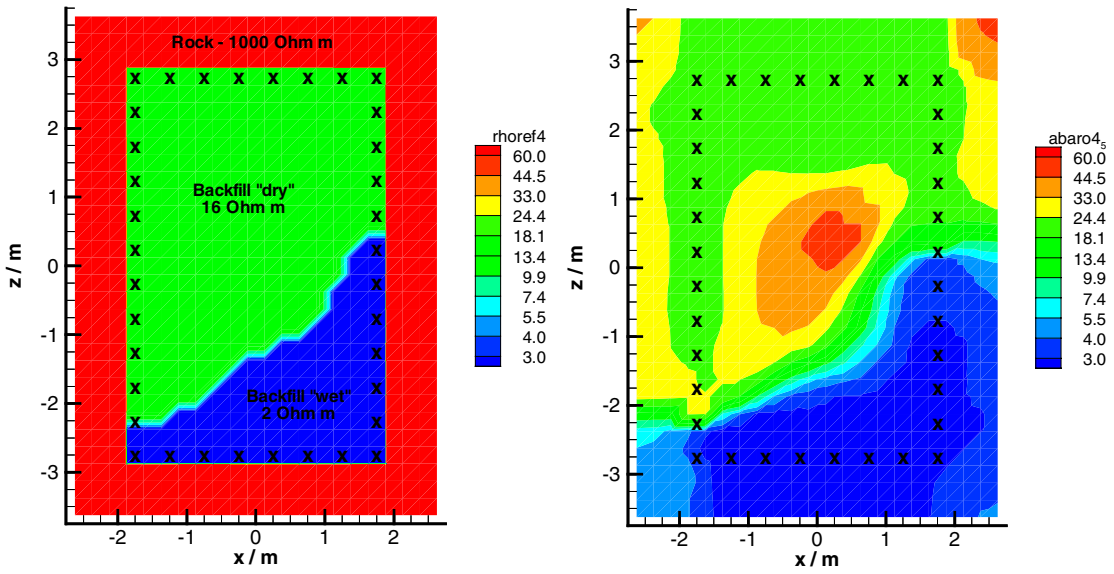

Figure 7-2: *Geoelectric modelling of the prototype repository backfill: Rectangular model with surrounding rock (left: input model, right: inversion result)*

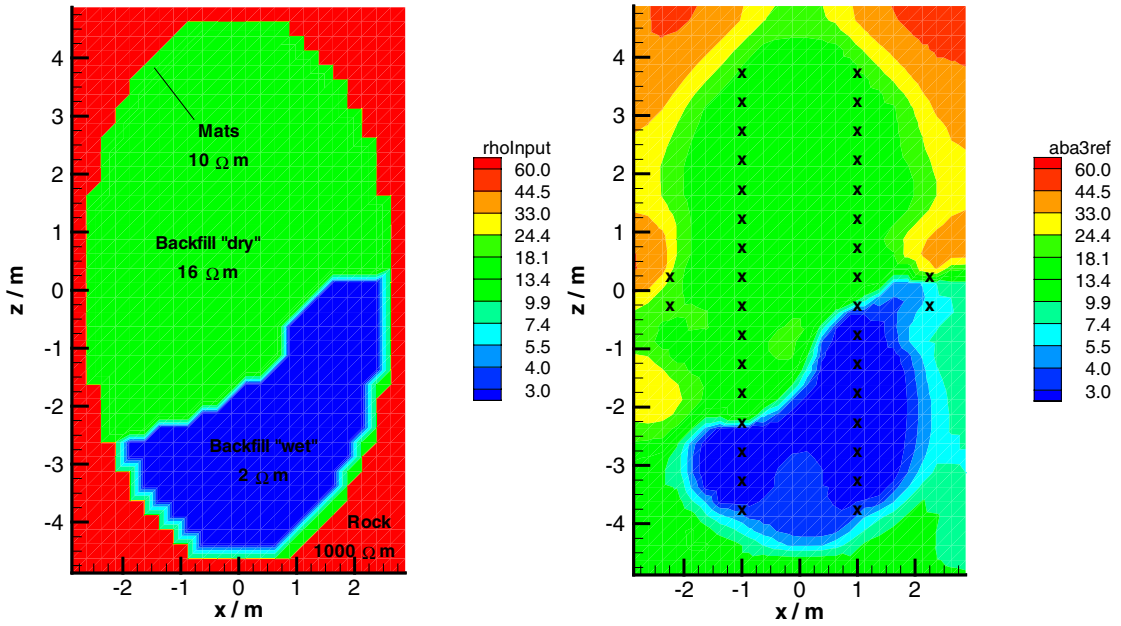

Figure 7-3: *Geoelectric modelling of the prototype repository backfill: Elliptic drift model with surrounding rock (left: input model, right: inversion result); "double cross" electrode arrangement (x = electrode locations)*

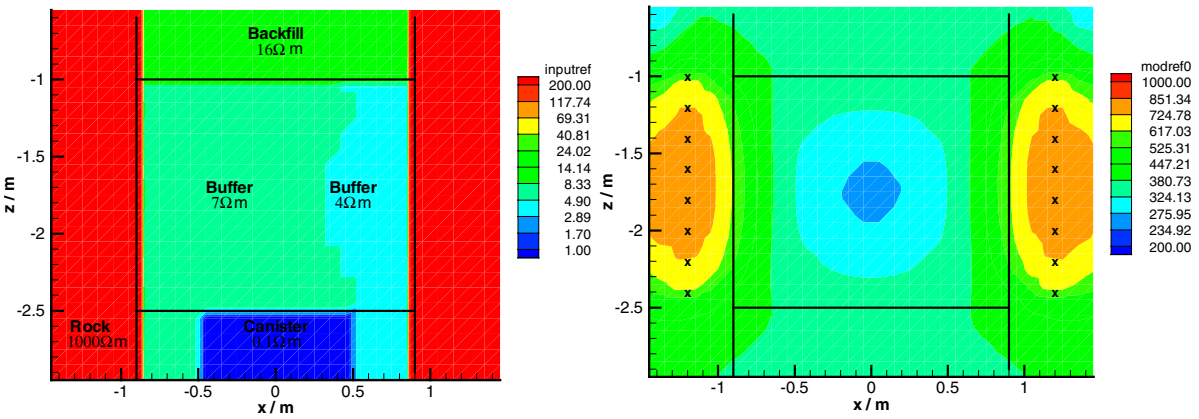

Figure 7-4: *Geoelectric modelling of the prototype repository buffer with the original electrode arrangement (left: input model, right: inversion result)*

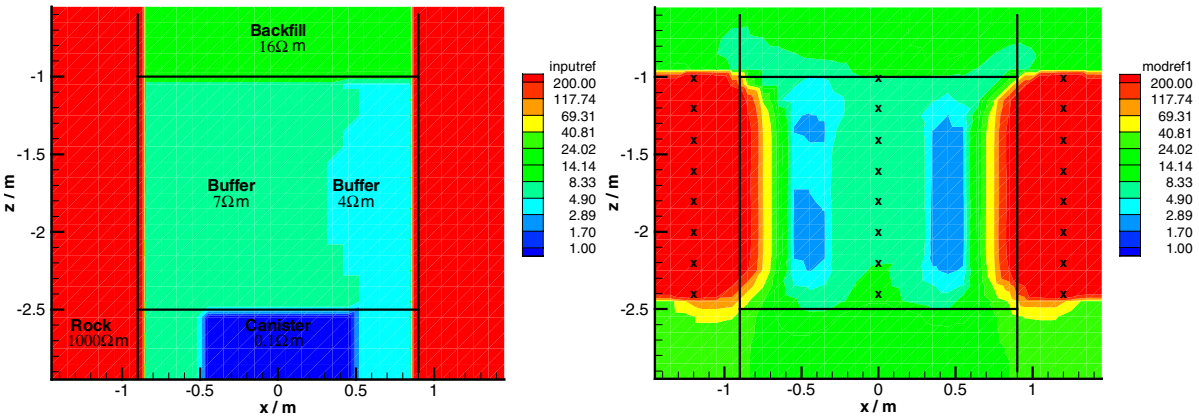

Figure 7-5: *Geoelectric modelling of the prototype repository buffer with additional central chain (left: input model, right: inversion result)*

In order to get a better resolution for the buffer resistivity distribution, a new electrode arrangement featuring two vertical chains in the buffer was agreed. One chain is to be placed near the centerline of the buffer and the other near the borehole wall. A third electrode chain in the rock at the original location is also kept.

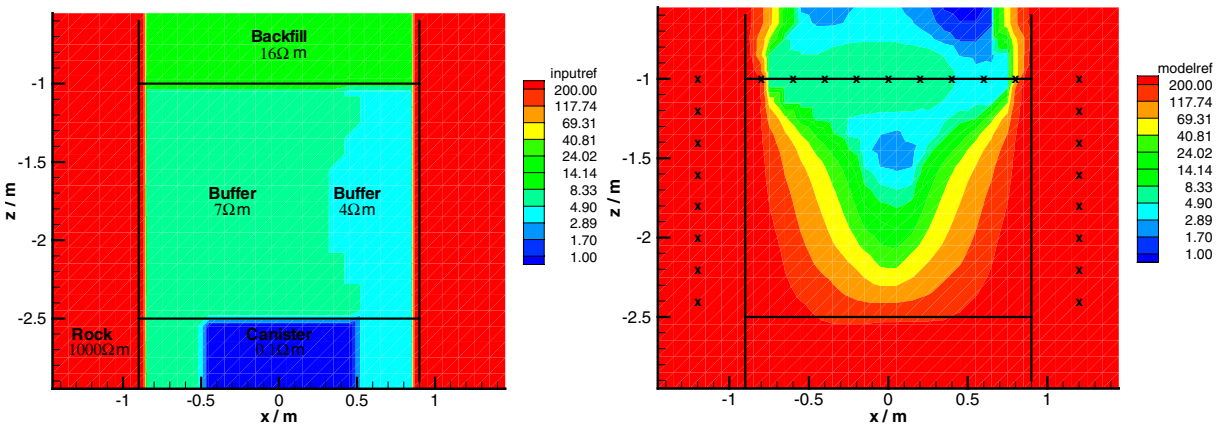

Figure 7-6: *Geoelectric modelling of the prototype repository buffer with additional horizontal chain (left: input model, right: inversion result)*

With this electrode arrangement a new modelling series was started. Figure 7-7 to Figure 7-9 show the results for a dry buffer, for a small wetted zone near the wall, and for an enlarged wetted zone.

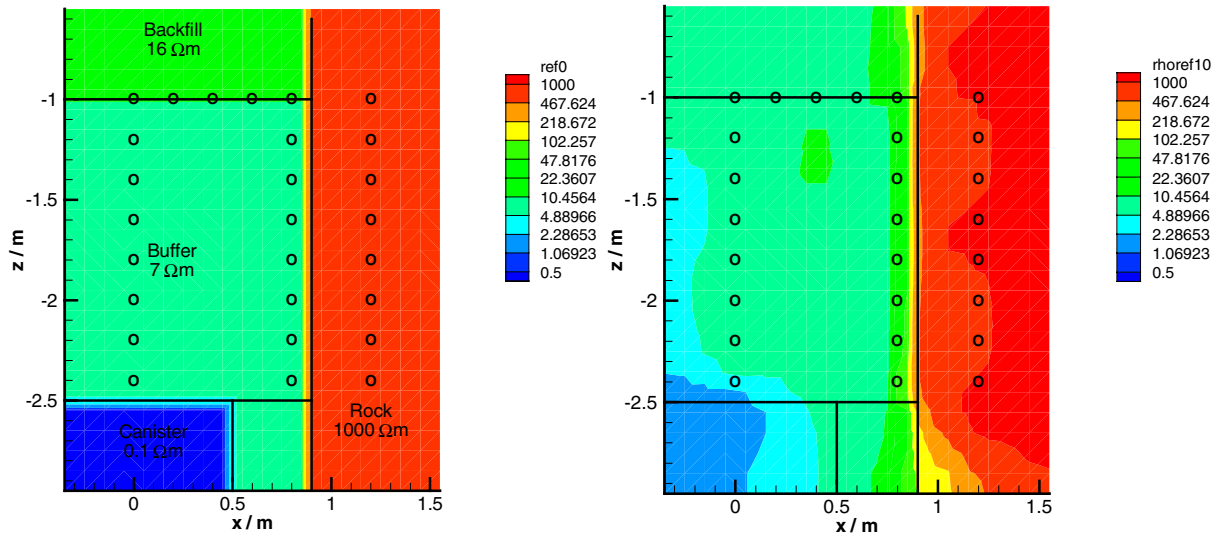

Figure 7-7: *Geoelectric modelling of the prototype repository buffer with the new electrode arrangement: dry buffer (left: input model, right: inversion result)*

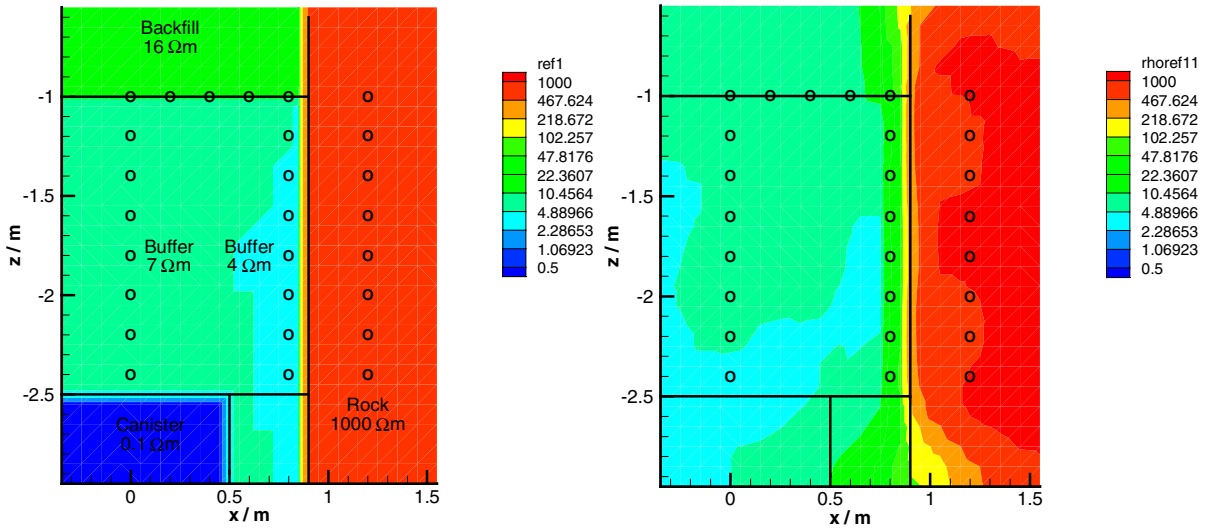

Figure 7-8: *Geoelectric modelling of the prototype repository buffer with the new electrode arrangement: partially wetted buffer (left: input model, right: inversion result)*

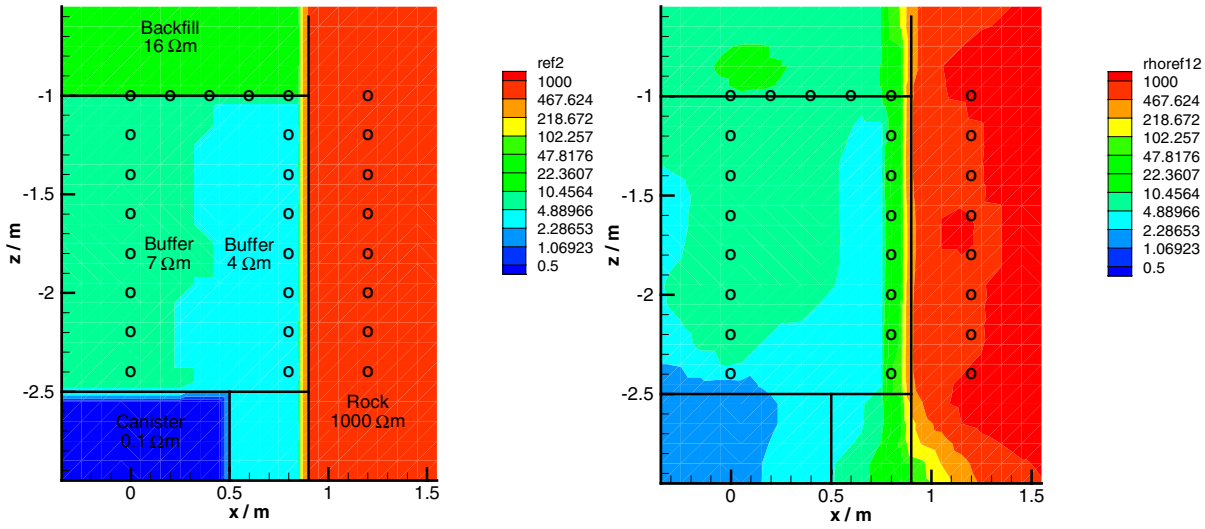

Figure 7-9: *Geoelectric modelling of the prototype repository buffer with the new electrode arrangement: enlarged wet buffer zone (left: input model, right: inversion result)*

The figures show that although there are some deviations from the input model, especially at the left model border and near the heater, the buffer resistivity distribution is fitted rather well. The most interesting region near the borehole wall is modelled in a reliable way. In particular, no high or low resistivity "ghosts" are generated, as for instance in Figure 7-5. Therefore, the new electrode arrangement appears adequate for the planned investigation.

8 Summary and Conclusions

For monitoring water uptake in buffer and backfill and saturation changes in the rock in the Prototype Repository the automatic measuring system RESECS has been purchased. Tomographic dipole-dipole measurements will be performed in four electrode arrays distributed in the drift backfill, in the buffer at top of borehole 5, and in the rock between boreholes 5 and 6. The electrode chains consist of water-tight ELOCAB cables and GISMA plugs as well as of electrodes manufactured in GRS's workshop in Braunschweig.

In order to interpret the measured resistivities in terms of water content the resistivities of compacted MX-80 samples and of drift backfill were determined by laboratory investigations. The resistivities were measured using the four-point method.

The resistivities of the original buffer material were not significantly different to the resistivities of the backfill. Both the compacted MX-80 bentonite and the backfill show a very similar steep drop of the resistivity at the lower water contents. This can be explained by a clay-typical interface conductivity which is due to additional cations held loosely in the diffuse part of the electrical double layer surrounding the clay particles. Already a small amount of solution leads to formation of a double layer and causes the interface conductivity. The relatively small resistivity changes observed at higher saturation indicate that the interface conductivity is the predominant part of the conductivity in MX-80 bentonite. Because of the similar behaviour, it is furthermore concluded that the bentonite governs the resistivity behaviour of the backfill.

According to the laboratory results, the buffer and backfill will have already a rather small resistivity of about 7 Ωm and 13 Ωm, respectively when installed (at a water content of 12 to 13 wt.%). In conjunction with the comparably high resistivity of the rock (approx. 1000 Ωm at full saturation) this may have the effect that resistivity reductions by increasing water uptake in the buffer cannot be properly detected if the electrodes are located in the rock or rather close to the rock. In order to clear this issue, model calculations were performed in order to determine optimum electrode arrangements enabling high resistivity resolution. As a result of the analyses the electrode arrangement in the drift backfill will be slightly changed. The measurements in the buffer at top of borehole 5 will now be performed by placing three electrode chains in the buffer and one chain in the rock.

Besides its dependence on the water content, the electrical resistivity is also a function of salinity and composition of the pore solution. Since both may change as the solution penetrates the buffer and the backfill, investigations were performed in order to quantify this effect.

For the investigation of solution composition changes during the penetration, Äspö-solution was applied to a 0.5 cm thin disk layer of compacted bentonite. In general it may be concluded that at the beginning of the experiment the sample takes up Mg and Ca from solution while Na and K are being released. Dissolution of some minor components of MX-80 was also observed in the experiments. As the normality of percolate remains to be higher than that of Äspö-solution, this process seemingly remains to continue during the whole experiment. It cannot be explained with cation exchange.

The observed slight increase in salinity compared to the initial value for Äspö-solution does not indicate a significant change of electrical conductivity. However, to quantify this effect respective measurements of electrical conductivity of the percolates obtained will be performed in the near future.

At the time of this report about 70 % of the preparatory works have been terminated. The monitoring equipment is ready for installation in the Prototype Repository. The laboratory calibrations will continue with further temperature dependent measurements for the backfill and the buffer as well as for the rock. This part of the work will be completed by mid 2002.

9 References

Benzel, W. M.; Graf, D. L. (1984): Studies of smectite membrane behaviour: Importance of layer thickness and fabric in experiments at 20°C, Geochim. Cosmochim. Acta (48), 1769-1778.

Dahlström, L.-O. (1998): Testplan for the Prototype Repository, Prpgress report HRL-98-24, Äspö Hard Rock Laboratory, SKB, Stockholm.

Demir, I. (a) (1988): Studies of smectite membrane behaviour: electrokinetic, osmotic and isotopic fractionation at elevated pressures, Geochim. Cosmochim. Acta (52), 727-737.

Demir, I. (b) (1988): The interrelation of hydraulic and electrical conductivities, streaming potential, and salt filtration during the flow of chloride brines through a smectite layer at elevated pressures, Journal of Hydrology (98), 31-52.

DIN 18121-1: Baugrund, Untersuchung von Bodenproben - Wassergehalt- Teil 1: Bestimmung durch Ofentrocknung, Normenausschuss Bauwesen (NABau) im DIN Deutsches Institut, Normen e.V., April 1989

Dresner, L.; Kraus, K. A. (1963): Ion exclusion and salt filtering with porous ion-exchange materials, J. Phys. Chem. (67), 990-996.

Hanshaw, B. B.; Coplen, T. B. (1973): Ultrafiltration by a compacted clay membrane. II - Sodium ion exclusion at various ionic strengths, Geochim. Cosmochim. Acta (37), 2311-2327.

HarbourDom GmbH: "RESITOMO – Programmpaket zur 2.5D Modellierung und 2D Inversion von DC-Widerstandsdaten, HarbourDom Consulting - Geophysikalische Forschungs- und Beratungsgesellschaft mbH, Köln, 1996

Ishiguro, M.; Matsuura, T.; Detellier, C. (1996): A study on the solute separation and the pore size distribution of a montmorillonite membrane, Sep. Sci. Technol. (31/4), 545-556.

Johnson, K. S. (1979): Ion association and activity coefficients in electrolyte solutions, Ph. D. Thesis, Oregon State University.

Johnson, K. S.(1981): The calculation of ion pair diffusion coefficients: a comment, Mar. Chem. (10), 195-208.

Kemper, W. D.; Evans, N. A. (1963): Movement of water as affected by free energy and pressure gradients III. Restriction of solutes by membranes, Soil Sci. Soc. Am. Proc. (27), 485-490.

Kemper, W. D.; Maasland, D. E. L. (1964): Reduction in salt content of solution on passing through thin films adjacent to charged surfaces, Soil Sci. Soc. Am. Proc. (28), 318-323.

Kharaka, Y. K.; Berry, F. A. F. (1973): Simultaneous flow of water and solutes through geological membranes - I. Experimental investigation, Geochim. Cosmochim. Acta (37), 2577-2603.

Kharaka, Y. K.; Smalley, W. C. (1976): Flow of water and solutes through compacted clays, Am. Assoc. Petr. Geol. Bull. (60/6), 973-980.

Kull, H.; Flach, D.; Graefe, V. (2001): Untersuchung physikalischer Prozesse und Parameter zum Fluid- und Gastransport im Nahbereich von Endlagern in einer homogenen granitischen Gesteinsmatrix, Abschlussbericht zum gleichnamigen Forschungsprojekt des BMFT, FKZ 02 E 8151 A8, Gesellschaft für Anlagen- und Reaktorsicherheit mbH, GRS-172.

Marshall, C. E. (1948): The electrochemical properties of mineral membranes. VIII The theory of selective membrane behaviour, J. Phys. Chem. (52), 1284-1295.

Serra, O.: Fundamentals of well-log interpretation. 1. The acquisition of well logging data. (Development in petroleum science 15A), Elesevier; Amsterdam – Oxford – New York – Tokyo 1984).

Schick, R. and Schneider, G. (1973): Physik des Erdkörpers – Eine Einführung für Naturwissenschaftler und Ingenieure, Ferdinand Enke Verlag Stuttgart.

Schopper, J. R.: Electrical conductivity of rock containing electrolytes. In: Landold-Börnstein, Numerical Data and Fuctional Relationships in Science and Technology. New Series edited by K.-H. Hellwege, Groupe V: Geosphysics and Space Research, Volume 1, Physical properties of Rocks, subvolume b, edited by G. Angenheiser., Springer-Verlag Berlin, Heidelberg, New York 1982

Sposito, G. (1989): The Chemistry of Soils, Oxford University Press.

Zimmer, U. (2001): In: Twophaseflow-Experiment in fractured crystalline rock, GRS-report, to be published.